iScience

CellPress
OPEN ACCESS

Article

# FAM134B deletion exacerbates apoptosis and epithelial-to-mesenchymal transition in rat lungs exposed to hyperoxia

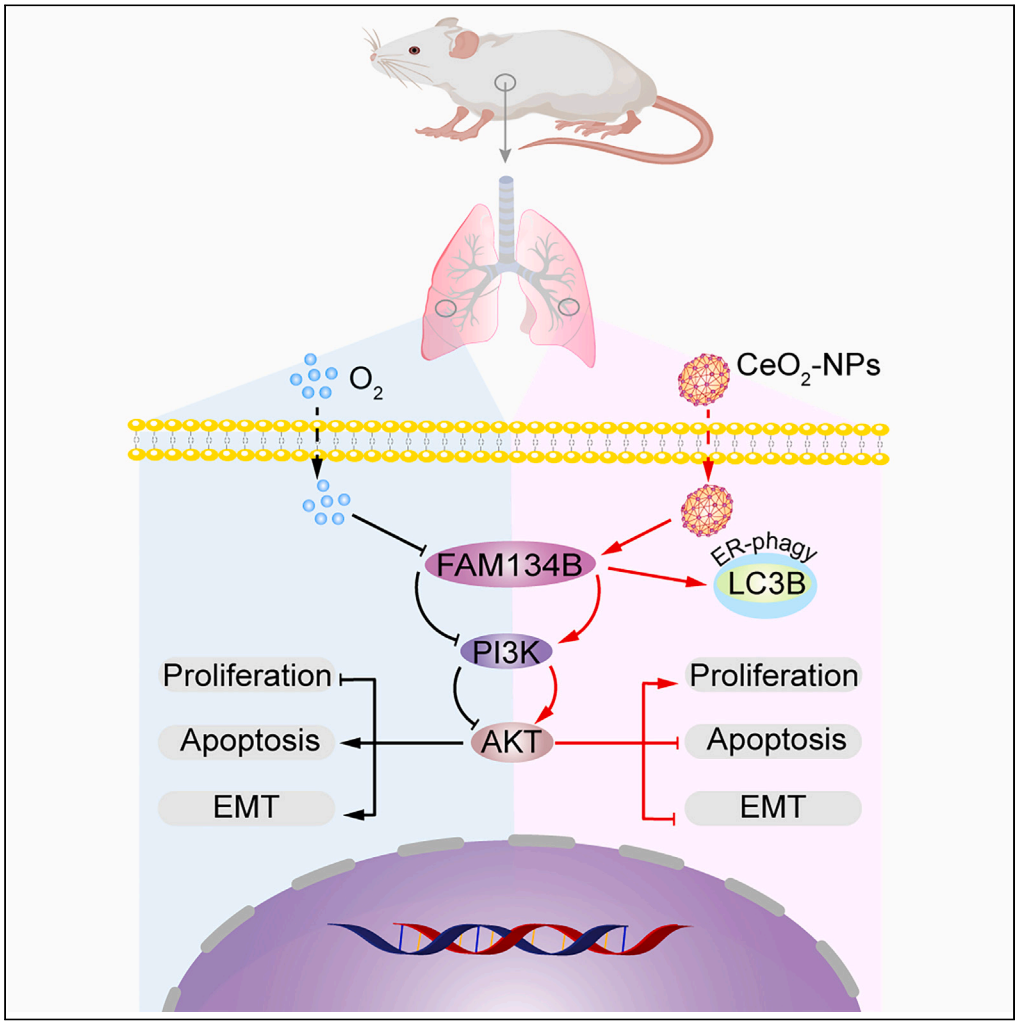


Hong Guo, Rong-Rong Huang, Shan-Shan Qu, Ying Yao, Su-Heng Chen, Shao-Li Ding, Yu-Lan Li

liyul@lzu.edu.cn

## Highlights

Deletion of FAM134B is responsible for hyperoxia-exposed lung injury

FAM134B protects hyperoxia-exposed lung injury via the PI3K/AKT pathway

$CeO_2$-NPs exert protective effects on hyperoxia-exposed lung by restoring ER-phagy

Guo et al., iScience *27*, 110385
July 19, 2024 
https://doi.org/10.1016/j.isci.2024.110385

iScience

CellPress
OPEN ACCESS

Article

# FAM134B deletion exacerbates apoptosis and epithelial-to-mesenchymal transition in rat lungs exposed to hyperoxia

Hong Guo,[1,2] Rong-Rong Huang,[1] Shan-Shan Qu,[1] Ying Yao,[1] Su-Heng Chen,[1] Shao-Li Ding,[1] and Yu-Lan Li[1,3,4,*]

## SUMMARY

**Oxygen therapy is widely used in clinical practice; however, prolonged hyperoxia exposure may result in hyperoxic acute lung injury (HALI). In this study, we investigated the role of FAM134B in hyperoxia-induced apoptosis, cell proliferation, and epithelial-to-mesenchymal transition (EMT) using RLE-6TN cells and rat lungs. We also studied the effect of $CeO_2$-NPs on RLE-6TN cells and lungs following hyperoxia exposure. FAM134B was inhibited in RLE-6TN cells and rat lungs following hyperoxia exposure. Overexpressing FAM134B promoted cell proliferation, and reduced EMT and apoptosis following hyperoxia exposure. FAM134B activation increased ER-phagy, decreased apoptosis, improved lung structure damage, and decreased collagen fiber deposition to limit lung injury. These effects could be reversed by PI3K/AKT pathway inhibitor LY294002. Additionally, $CeO_2$-NPs protected RLE-6TN cells and lung damage following hyperoxia exposure by ameliorating impaired ER-phagy. Therefore, FAM134B restoration is a potential therapeutic target for the HALI. Moreover, $CeO_2$-NPs can be used for the treatment of HALI.**

## INTRODUCTION

Oxygen therapy is extensively used in pulmonary disease and critical care resuscitation. However, prolonged exposure to high concentrations of oxygen may cause oxygen toxicity, leading to hyperoxic acute lung injury (HALI) and increased mortality.[1–4] The development of HALI involves excessive ROS production and the release of inflammatory mediators, which induce lung epithelial cell apoptosis or necrosis.[5]

Alveolar type II epithelial cells (AEC2s) are progenitor cells that repair lung injury and maintain alveolar homeostasis. Hyperoxia-induced damage to AEC2s causes HALI, which induces lung tissue fibrosis via epithelial-to-mesenchymal transition (EMT).[6,7] Lung alveolar epithelial cells differentiate into myofibroblasts, which repair damaged tissue by fibrosis, via hyperoxia-induced EMT.[8,9] EMT, increased apoptosis, and decreased cell proliferation of AEC2s are key factors contributing to HALI.[7,10] However, the mechanisms underlying these factors remain unclear, and effective therapeutic strategies are limited.

The endoplasmic reticulum (ER), where proteins and lipids are mainly synthesized, is involved in cell remodeling via ER stress-activated autophagy or selective ER phagocytosis.[11] The ER undergoes continuous remodeling via a selective autophagy pathway, known as ER-phagy. It was reported that hyperoxia impairs ER homeostasis in alveolar epithelial cells, resulting in HALI[12]; and ER homeostasis is restored in neurons by promoting ER-phagy, thereby inhibiting neuronal apoptosis.[13] What is the role of ER-phagy in the development of HALI, and how the process of HALI may be influenced by interfering with ER-phagy? That is an open question.

When MAP1LC3B binds to FAM134B, an ER-phagy receptor, ER fragments are degraded by selective autophagy, and ER homeostasis is maintained,[14,15] preserving cellular function. FAM134B-mediated ER-phagy results from the activation of the ROS pathway by advanced glycation end products (AGEs). FAM134B overexpression attenuates AGE-induced intracellular ROS accumulation, apoptosis, and senescence, which are reversed by FAM134B knockdown.[16] Further, FAM134B overexpression attenuated epilepsy-induced ROS levels and apoptosis in hippocampal neurons.[17] FAM134B deficiency reduced cell proliferation in breast cancer cells.[18] However, whether FAM134B-mediated ER-phagy affects hyperoxia-induced alveolar epithelial cell injury remains unknown.

Cerium oxide nanoparticles ($CeO_2$-NPs), which possess reversible redox properties due to the interconvertibility between $Ce^{3+}$ and $Ce^{4+}$,[19,20] can scavenge multiple ROS[21,22] and be used to treat oxidative stress-related diseases. Although $CeO_2$-NPs can reduce hepatic steatosis[23] and exert antitumor effects,[24] the biomedical mechanism underlying its effects against HALI remains unknown.

Here, we verified the role of FAM134B in hyperoxia-induced apoptosis, inhibiting cell proliferation, and EMT, as well as the biomedical effects exerted by $CeO_2$-NPs. In addition, we investigated, for the first time, the mechanisms by which $CeO_2$-NPs protects against HALI.

[1]First Clinical Medical College, Lanzhou University, Lanzhou 730000, China
[2]Department of Anesthesiology, Inner Mongolia Hospital of Peking University Cancer Hospital, Affiliated People's Hospital , Inner Mongolia Medical University, Hohhot 10020, China
[3]Department of Anesthesiology, First Hospital of Lanzhou University, Lanzhou University, Lanzhou 730000, China
[4]Lead contact
*Correspondence: liyul@lzu.edu.cn
https://doi.org/10.1016/j.isci.2024.110385

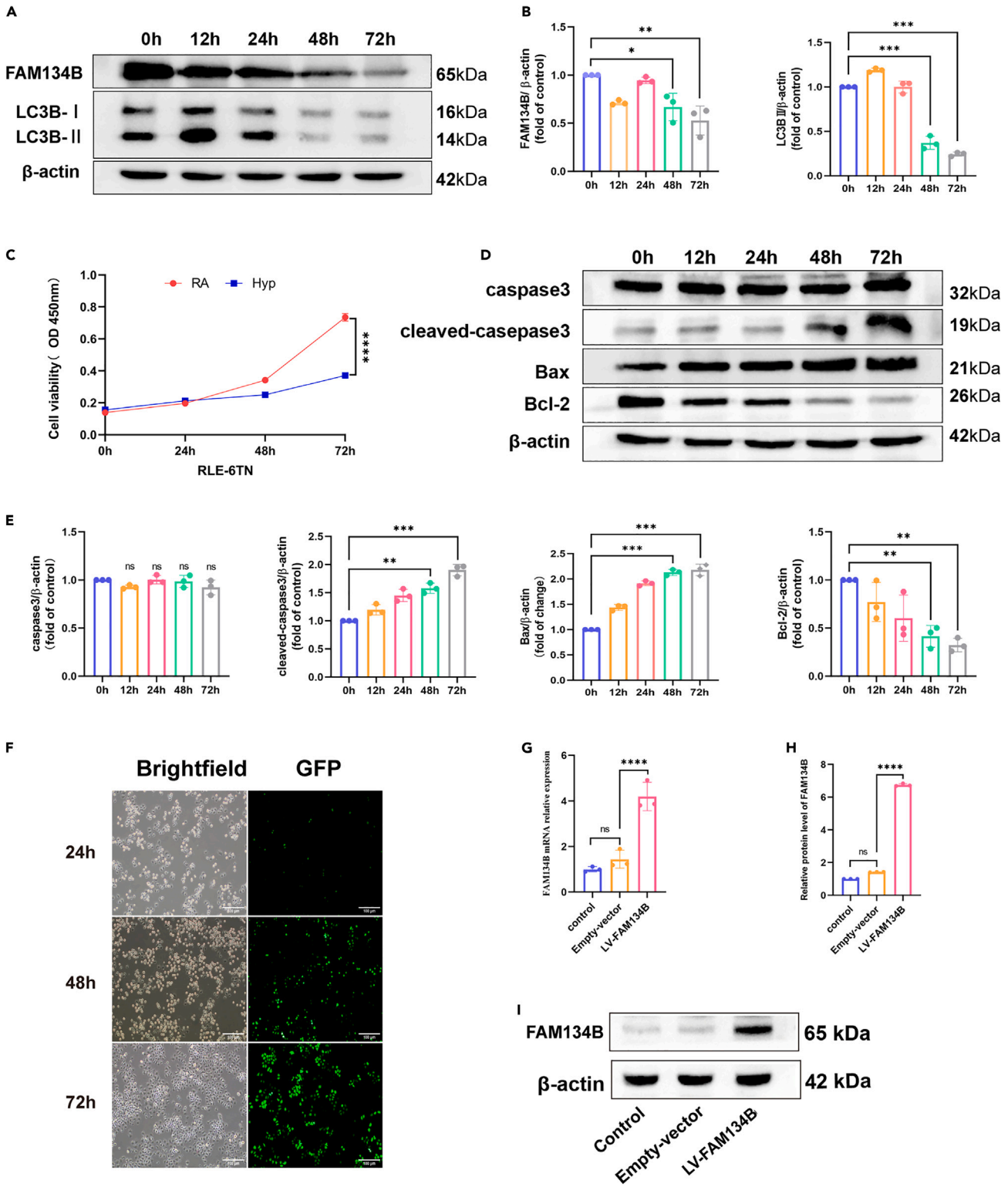


**Figure 1. Hyperoxia exposure inhibits ER-phagy, suppresses cell proliferation, and promotes apoptosis in AEC2s cells**

(A) Western blot analysis of FAM134B and LC3B following the exposure of RLE-6TN cells to 95% hyperoxia.

(B) Optical density analysis of FAM134B and LC3B (±SD, *n* = 3).

(C) CCK8 assessment of cell proliferation of RLE-6TN cells exposed to 95% hyperoxia and air groups; RA: room air group; Hyp: hyperoxia group (±SD, *n* = 3).

**Figure 1. *Continued***

(D) Western blot analysis of caspase3, cleaved-caspase3, Bax, and Bcl-2 in RLE-6TN cells after exposure to 95% hyperoxia.

(E) Optical density analysis of caspase3, cleaved-caspas3, Bax, and Bcl-2 (±SD, $n = 3$).

(F) Green GFP fluorescence in lentivirus-transfected RLE-6TN cells (scale bar: 100 μm).

(G) The expression of mRNA after lentiviral transfection overexpressing FAM134B (±SD, $n = 3$).

(H) Optical density analysis of FAM134B after lentiviral transfection overexpressing FAM134B (±SD, $n = 3$).

(I) Western blot detected the protein expression level of FAM134B after lentiviral transfection overexpressing FAM134B. *$p < 0.05$; **$p < 0.01$; ***$p < 0.001$,****$p < 0.0001$.

## RESULTS

### Hyperoxia exposure inhibits ER-phagy, suppresses cell proliferation, and promotes apoptosis in AEC2s

First, we evaluated the effect exerted by different periods of hyperoxia exposure on RLE-6TN. We exposed RLE-6TN cells to 95% hyperoxia for 0, 12, 24, 48, and 72 h. During autophagy, LC3B-I is converted to LC3B-II; therefore, reduced LC3B-II expression indicates reduced autophagic flux.[25] We found that the total expression of the autophagy marker protein LC3B-II, and expression of FAM134B were reduced in a time-dependent manner during exposure to hyperoxia. The expression levels of LC3B-II and FAM134B were significantly reduced after 48 h of exposure to hyperoxia (Figures 1A and 1B). The viability of RLE-6TN cells in the hyperoxia (Hyp) group was significantly inhibited compared with that of cells in the normoxia group (RA group) (Figure 1C). Western blotting indicated that in RLE-6TN cells exposed to 95% hyperoxia, cleaved-caspase3, and Bax expression gradually increased, whereas Bcl-2 expression decreased (Figures 1D and 1E). Based on the previous results, 48 h was selected as the time point for hyperoxia exposure for the following experiment.

To determine whether restoration of ER-phagy would reverse hyperoxia-induced damage to AEC2s, we transfected RLE-6TN cells using FAM134B lentivirus and observed the transfection levels of lentivirus using fluorescence microscopy. Successful transfection is shown as green fluorescence in Figure 1F. FAM134B mRNA (Figure 1G) and protein expression levels (Figures 1H and 1I) were detected following the transfection of RLE-6TN cells with lentivirus. The results showed that FAM134B mRNA and protein levels in the LV-FAM134B group were significantly higher than those in the other groups after 72 h, whereas the differences between the control and empty vector groups were not statistically significant. This finding demonstrated that FAM134B-overexpressing RLE-6TN cells were successfully established. We further investigated whether restoring ER-phagy with hyperoxia would affect apoptosis, proliferation, or migration of AEC2s.

### FAM134B overexpression restored ER-phagy, increased cell viability, reduced apoptosis, and inhibited EMT in hyperoxia-exposed AEC2s

Overexpression of FAM134B significantly increased the level of impaired ER-phagy following exposure to hyperoxia, as evidenced by increased LC3B-II expression (Figures 2A and 2B). It also significantly attenuated apoptosis, resulting in decreased cleaved-caspase 3 and Bax expression and increased Bcl-2 expression (Figures 2A and 2B). Overexpression of FAM134B significantly attenuated apoptosis (Figures 2C and 2D) and increased the proliferation of RLE-6TN cells following exposure to hyperoxia (Figure 2E).

EMT results in the development of pulmonary fibrosis, which essentially involves tissue damage due to persistent inflammation.[26] In the present study, hyperoxia exposure promoted the development of EMT in RLE-6TN cells, as evidenced by decreased E-cadherin expression and increased N-cadherin and Vimentin expression, whereas overexpression of FAM134B significantly reversed EMT in RLE-6TN cells that had been exposed to hyperoxia (Figures 2F and 2G). Migration of lung epithelial cells to the interstitial region and alveolar lumen is an important step in EMT development.[27] Therefore, we analyzed the effect of FAM134B overexpression on the migratory ability of RLE-6TN cells using transwell and wound-healing assays. The results indicated that hyperoxia promoted cell migration of RLE-6TN, and the overexpression of FAM134B effectively prevented hyperoxia-induced cell migration (Fig. 2H–K).

### PI3K/AKT pathway was inhibited by hyperoxia and activated by FAM134B overexpression

Activation of the PI3K/AKT pathway is associated with increased cellular glucose metabolism and increased survival.[28,29] To identify the pathways associated with hyperoxia-induced lung injury, we analyzed the microarray dataset, GSE125489 (global gene expression changes in the lung of hyperoxia-exposed mice), from the Gene Expression Omnibus (GEO) database. Differentially expressed genes (DEGs) were identified, and the Database for Annotation, Visualization, and Integrated Discovery (DAVID) was used for Gene Ontology (GO) and Kyoto Encyclopedia of Genes and Genomes (KEGG) pathway analyses. The PI3K/AKT pathway appeared in the enrichment results (Figure 3A), and key genes in the pathway such as CD19, ERBB2, FGF22, ITGA11, KDR, NTRK2, PDGFRA, PKN1, RPS6 were downregulated (Figure 3B). Hyperoxia inhibits the PI3K/AKT pathway, while the activation of the pro-survival factor AKT prevents AEC2s damage in rats subjected to oxygen-induced lung injury.[30] The results of our study indicated that FAM134B overexpression significantly activated the PI3K/AKT pathway, which had been inhibited by hyperoxia exposure (Figures 3C and 3D).

### Inhibition of the PI3K/AKT pathway by LY294002 reversed increased cell viability and reduced apoptosis and EMT inhibition in RLE-6TN cells overexpressing FAM134B

To investigate the role of PI3K/AKT in the protective effect exerted by FAM134B on hyperoxia-exposed RLE-6TN cells, we used a PI3K/AKT pathway inhibitor, LY294002, and monitored changes in apoptosis, proliferation, and EMT in RLE-6TN cells. LY294002 significantly inhibited

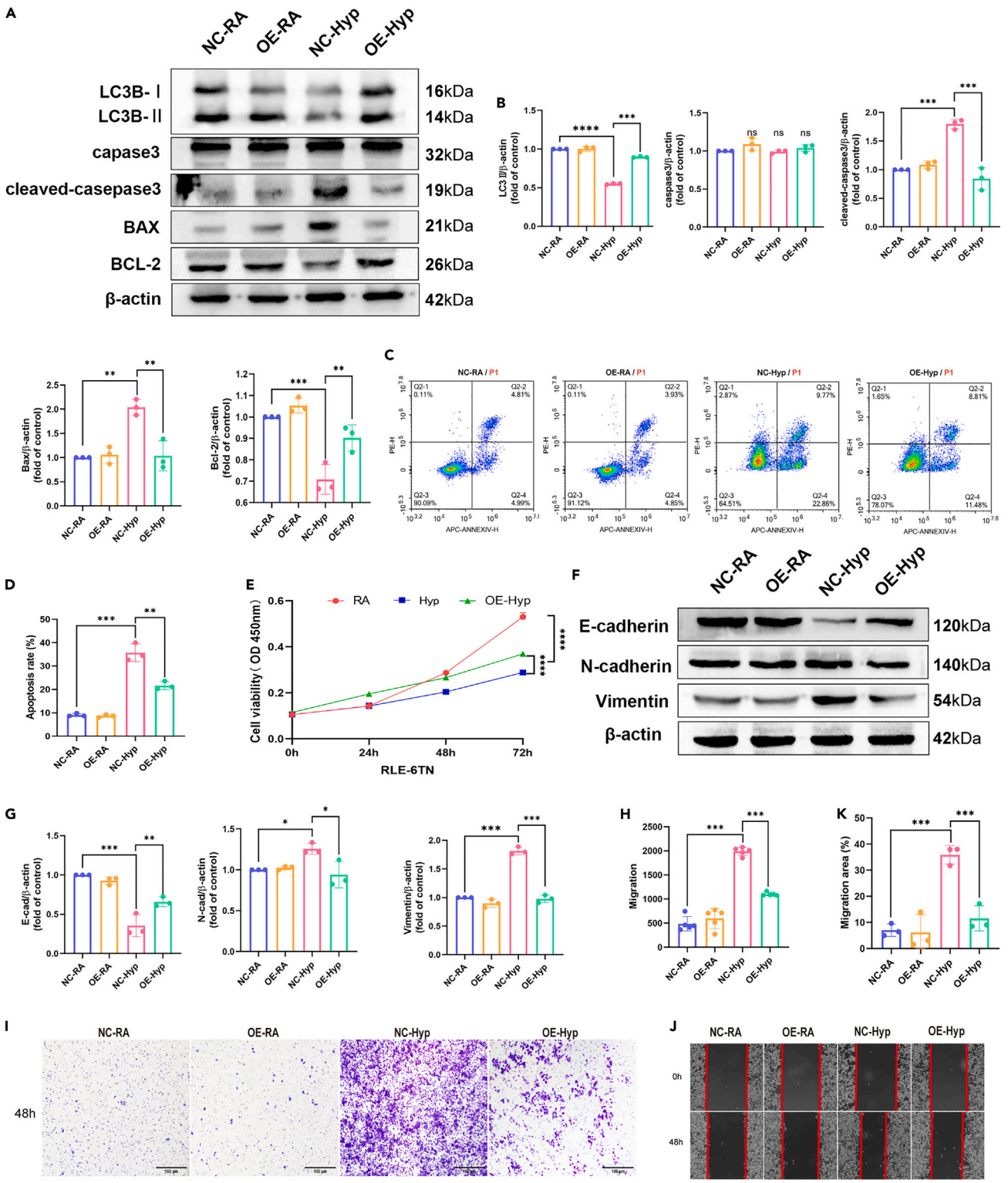


**Figure 2. FAM134B overexpression restored ER-phagy, increased cell viability, reduced apoptosis, and inhibited EMT in hyperoxia-exposed AEC2s cells**

(A) Western blot analysis of LC3B, caspase3, cleaved-caspase3, Bax, and Bcl-2 in RLE-6TN cells after overexpression of FAM134B.

**Figure 2. *Continued***

(B) Optical density analysis of LC3B, caspase3, cleaved-caspase3, Bax, and Bcl-2 (±SD, $n = 3$).

(C) Flow cytometry determination of apoptosis in each group.

(D) Quantitative analysis of flow cytometry results (±SD, $n = 3$).

(E) CCK8 assessment of the effect of overexpression of FAM134B on cell proliferation exposed to 95% hyperoxia or air (±SD, $n = 3$).

(F) Western blot analysis of E-cadherin, N-cadherin, and Vimentin in RLE-6TN cells after overexpression of FAM134B.

(G) Optical density analysis of E-cadherin, N-cadherin, and Vimentin (±SD, $n = 3$).

(H) Quantification of migrating cells was performed in transwell chambers (±SD, $n = 5$).

(I) RLE-6TN cells were visualized using phase-contrast microscopy for the analysis of migration ability (100× magnification; scale bar: 100 μm).

(J and K) A 48-h incubation period for RLE-6TN cells was followed by a wound-healing test (±SD, $n = 3$). RA: room air group; Hyp: hyperoxia group; NC: empty vector group; OE: FAM134B overexpression group; $^{*}p < 0.05$, $^{**}p < 0.01$, $^{***}p < 0.001$, $^{****}p < 0.0001$.

the effect of FAM134B overexpression on the activation of the PI3K/AKT pathway in cells exposed to hyperoxia (Figures 3E and 3F). LY294002 reversed the reduction in apoptosis (Figures 3E and 3F; Figures 4A and 4B) and the increase in cell proliferation (Fig. 4C–E) induced by FAM134B overexpression following hyperoxia exposure. Hyperoxia promoted EMT in RLE-6TN cells, as evidenced by decreased E-cadherin expression and increased N-cadherin and Vimentin expression. Overexpression of FAM134B reduced EMT induced by hyperoxia, and LY294002 reversed the beneficial reduction in EMT induced by FAM134B overexpression (Figures 4F and 4G). Transwell and wound-healing assays confirmed that hyperoxia promoted the migration of RLE-6TN cells, whereas overexpression of FAM134B effectively prevented hyperoxia-induced migration of RLE-6TN cells. However, LY294002 reversed the beneficial reduction in cell migration induced by the overexpression of FAM134B following exposure to hyperoxia (Fig. 4H–K).

## $CeO_2$-NPs reduced apoptosis, decreased EMT, and increased the cell viability of AEC2s cells following hyperoxia exposure, thereby protecting against the impairment of autophagy levels following hyperoxia exposure

First, we observed the properties of $CeO_2$-NPs using electron microscopy (Figures 5A and 5B). Consistent with the manufacturer's description, the product showed good dispersion with a nanoparticle size of 3–5 nm. We then evaluated the effects of different concentrations of $CeO_2$-NPs on cell proliferation using CCK8 and live cell imaging, and the results showed that none of the concentrations in the range of 0–20 μg/mL either exerted any toxic effects on cells or affected cell proliferation (Figures 5C and 5D). For subsequent experiments, we used a dose of 10 μg/mL. The valence conversion from $Ce^{3+}$ to $Ce^{4+}$ in $CeO_2$-NPs provides them with the properties of nano-enzyme, which is similar to the mechanism of action of various oxidoreductases that catalyze redox reactions in cells and tissues.[31] $CeO_2$-NPs exerted a significant ROS scavenging effect on hyperoxia-exposed cells as detected by the DCFH-DA probe (Figures 5E and 5F). Further, $CeO_2$-NPs reduced apoptosis (Figure 5G, H, J, K) and EMT following hyperoxia exposure (Figures 5H and 5I).

Transwell and wound-healing assays showed that $CeO_2$-NPs reversed hyperoxia-induced enhancement of cell migration (Fig. 6A–D) and increased hyperoxia-exposed cell viability (Fig. 6E–G). $CeO_2$-NPs also exerted a protective effect on the inhibition of ER-phagy levels following hyperoxia exposure, as evidenced by the reduced downregulation of FAM134B and LC3B-II in cells following hyperoxia exposure (Fig. 6H–J). The previous results indicated that $CeO_2$-NPs may exert a protective effect on hyperoxia-exposed RLE-6TN cells by protecting ER-phagy via the attenuation of FAM134B downregulation.

To determine whether the protective effect of FAM134B is also relevant *in vivo*, we performed a comparative study in Sprague-Dawley rat lungs and explored the role of $CeO_2$-NPs in HALI.

## Overexpression of FAM134B in Sprague-Dawley rat lung tissues activates P-AKT and attenuates HALI, whereas LY294002 reverses these effects

First, overexpression of FAM134B was significantly inhibited following hyperoxia exposure (Figure 7A). P-AKT was inhibited in rats following hyperoxia exposure, and overexpression of FAM134B promoted P-AKT activation. LY294002 reversed the promotion of P-AKT after FAM134B overexpression (Figure 7A). The lung tissues of rats in the hyperoxia group showed obvious damage, which manifested as thickening of the alveolar wall, extensive widening of the alveolar septum, congestion and exudation of the alveolar lumen, and infiltration of inflammatory cells. Lung injury was significantly reduced in the rats with overexpressed FAM134B, whereas the beneficial effect after FAM134B overexpression was reversed by LY294002 (Figure 7B). Hyperoxia induced collagen fiber deposition in rat lung tissues, and overexpression of FAM134B attenuated collagen fiber deposition, whereas collagen fiber deposition was aggravated in lung tissues after LY294002 treatment (Figure 7B). The wet/dry weight ratio of rats was significantly high following hyperoxia exposure, which decreased after overexpression of FAM134B, while the beneficial effects of FAM134B were attenuated after LY294002 treatment (Figure 7C). Overexpression of FAM1134B promotes ER-phagy activation (Figure 7D). We observed that the ER-phagy marker FAM134B colocalized with LC3B and presented as positive spots upon immunofluorescence staining (Figure 7E). This finding revealed that LC3B and FAM134B were expressed in the ER, with LC3B upregulation upon FAM134B overexpression (Figures 7E and 7F).

Our study indicated that FAM134B overexpression significantly activated the PI3K/AKT pathway, which had been inhibited by hyperoxia exposure in rat lung (Figure 8A). Hyperoxia increased apoptosis (Fig. 8B-D) and EMT (Figure 8E) in rat lung tissues, and overexpression of FAM134B attenuated these adverse effects following exposure to hyperoxia, while apoptosis was aggravated in lung tissues along with increased EMT after LY294002 treatment.

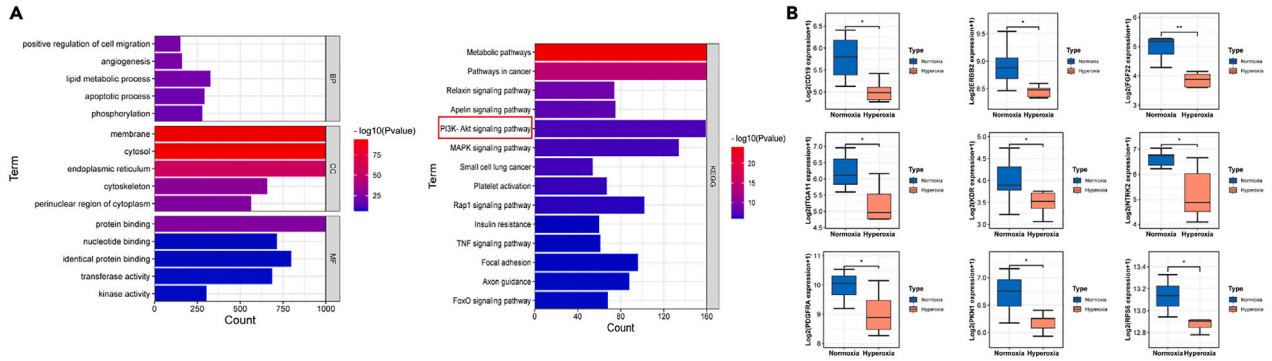
A
positive regulation of cell migration
angiogenesis
lipid metabolic process
apoptotic process
phosphorylation
membrane
cytosol
endoplasmic reticulum
cytoskeleton
perinuclear region of cytoplasm
protein binding
nucleotide binding
identical protein binding
transferase activity
kinase activity
BP
CC
MF
Term
Count
- log10(Pvalue)
Metabolic pathways
Pathways in cancer
Relaxin signaling pathway
Apelin signaling pathway
PI3K- Akt signaling pathway
MAPK signaling pathway
Small cell lung cancer
Platelet activation
Rap1 signaling pathway
Insulin resistance
TNF signaling pathway
Focal adhesion
Axon guidance
FoxO signaling pathway
KEGG
B
Type
Normoxia
Hyperoxia

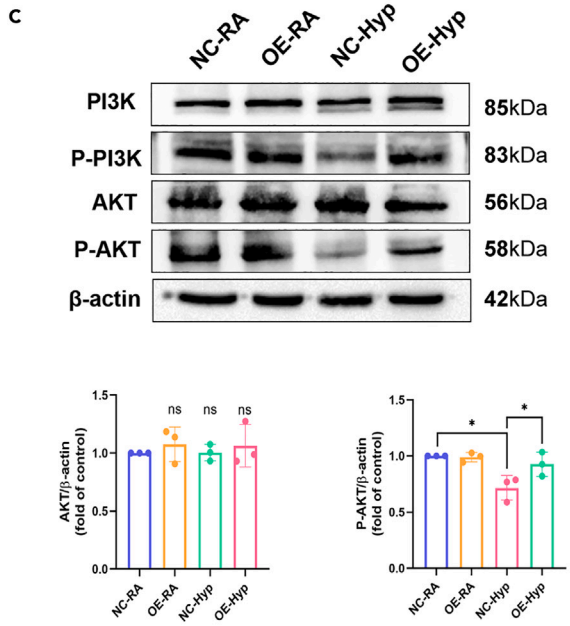
C
NC-RA
OE-RA
NC-Hyp
OE-Hyp
PI3K
P-PI3K
AKT
P-AKT
β-actin
85kDa
83kDa
56kDa
58kDa
42kDa
AKT/β-actin (fold of control)
P-AKT/β-actin (fold of control)
ns
*

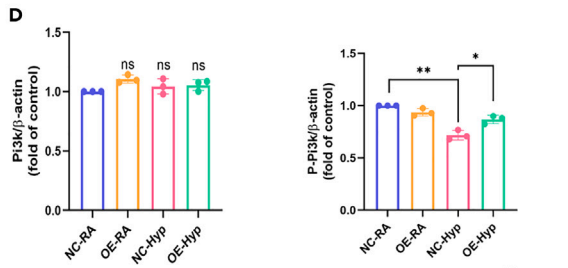
D
Pi3k/β-actin (fold of control)
P-Pi3k/β-actin (fold of control)
ns
**
*

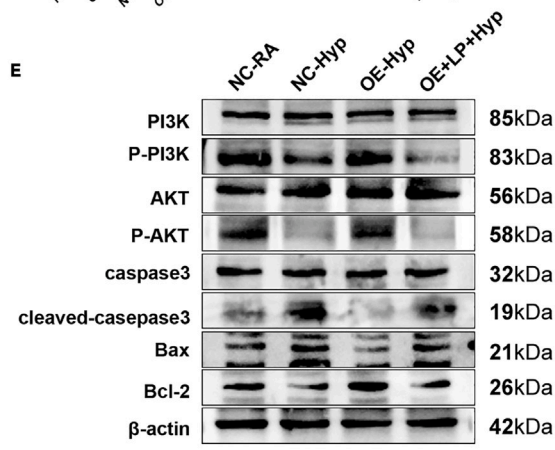
E
NC-RA
NC-Hyp
OE-Hyp
OE+LP+Hyp
PI3K
P-PI3K
AKT
P-AKT
caspase3
cleaved-casepase3
Bax
Bcl-2
β-actin
85kDa
83kDa
56kDa
58kDa
32kDa
19kDa
21kDa
26kDa
42kDa

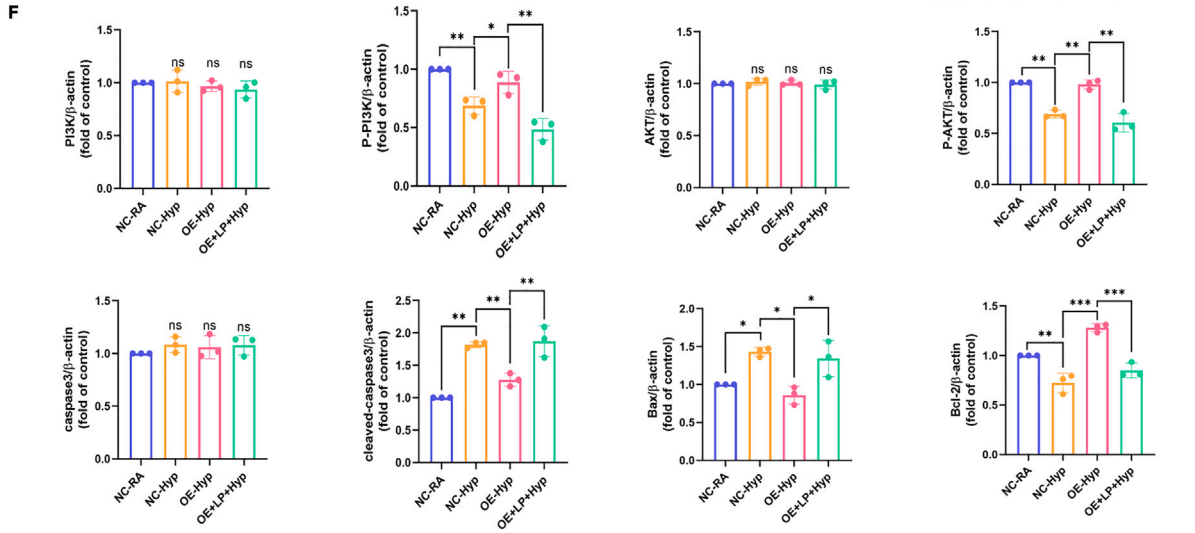
F
PI3K/β-actin (fold of control)
P-PI3K/β-actin (fold of control)
AKT/β-actin (fold of control)
P-AKT/β-actin (fold of control)
caspase3/β-actin (fold of control)
cleaved-caspase3/β-actin (fold of control)
Bax/β-actin (fold of control)
Bcl-2/β-actin (fold of control)
ns
*
**
***

**Figure 3. Hyperoxia inhibited the PI3K/AKT pathway whereas overexpression of FAM134B activated the PI3K/AKT pathway**

(A) Functional and pathway enrichment results of hyperoxia-exposed lung tissue (GSE125489 dataset).

(B) Expression of key genes in the pathway.

(C) Western blot analysis of PI3K, P-PI3K, AKT, and P-AKT in RLE-6TN cells following overexpression of FAM134B.

(D) Optical density analysis of PI3K, P-PI3K, AKT, and P-AKT (±SD, $n = 3$).

(E) Western blot analysis of PI3K, P-PI3K, AKT, P-AKT, caspase3, cleaved-caspase3, Bax, and Bcl-2 in RLE-6TN cells overexpressing FAM134B exposed to hyperoxia and treated with LY294002.

(F) Optical density analysis of PI3K, P-PI3K, AKT, P-AKT, caspase3, cleaved-caspase3, Bax, and Bcl-2 (±SD, $n = 3$). RA: room air group; Hyp: hyperoxia group; NC: empty vector group; OE: FAM134B overexpression group; LP: LY294002 group; $^{*}p < 0.05$, $^{**}p < 0.01$, $^{***}p < 0.001$.

### $CeO_2$-NPs attenuates lung injury and inhibits hyperoxia-induced downregulation of FAM134B in SD rats

Compared with the hyperoxia group, $CeO_2$-NPs treatment significantly alleviated hyperoxia-induced lung injury and collagen fiber deposition (Figure 9A). In addition, $CeO_2$-NPs significantly reduced the lung wet/dry weight ratio in rats following hyperoxia exposure (Figure 9B). Furthermore, $CeO_2$-NPs treatment significantly attenuated apoptosis (Figures 9C and 9D) and EMT (Figure 10A) in rat lung tissue following hyperoxia exposure.

To further investigate the mechanism of the protective effect of $CeO_2$-NPs against lung injury in rats, we examined the expression of FAM134B in rat lung tissues after treatment with $CeO_2$-NPs, and the results showed that $CeO_2$-NPs treatment partially restored the downregulated FAM134B following hyperoxia exposure (Figure 10B). $CeO_2$-NPs restored the deletion of FAM134B and LC3B following hyperoxia exposure (Figures 10C and 10D).

## DISCUSSION

Prolonged inhalation of high concentrations of oxygen may cause lung injury, and eventually HALI. In a previous study, we investigated the mechanism underlying HALI and potential protective strategies.[32] Autophagy is an essential survival mechanism adopted by cells subjected to starvation or stressful conditions.[33,34] In recent years, the role of organelle-specific autophagy in the stress response has received significant attention. The ER, which is the largest intracellular membrane structure, synthesizes proteins and lipids and maintains ionic homeostasis. ER-phagy regulates the shape, size, and function of its contents, which constitute an important aspect of cellular adaptation to stress response.[35] FAM134B is the first mammalian ER-phagy receptor to be identified.[36] In the present study, we investigated the role of FAM134B in AEC2s and rat lung tissues exposed to hyperoxia. To the best of our knowledge, this study is the first to report and provide direct evidence that FAM134B is downregulated in hyperoxia-exposed AEC2s and rat lung tissues. When overexpressed, FAM134B, an ER-resident receptor, directly interacts with the autophagy modifier, LC3B, and promotes ER-phagy to maintain ER degradation and ensure cellular homeostasis.[37] In our study, overexpression of FAM134B in RLE-6TN cells and rat lung tissues upregulated LC3B expression. Elevated LC3B levels are reportedly associated with the initiation of autophagy.[38] We suggest that overexpression of FAM134B induces the initiation of ER-phagy, which protects cells and lung tissue against damage caused by hyperoxia exposure; this was evidenced by increased LC3B expression, which decreased apoptosis and lung tissue damage induced by hyperoxia exposure and promoted cell proliferation. Moreover, the results of our study are consistent with those of a recent study that found that hyperoxia inhibited cellular autophagic flux in AEC2s, and partial restoration of autophagic flux increased the survival of AEC2s exposed to hyperoxia.[39]

EMT is a biologically important tissue remodeling process, and such transformation of the terminally differentiated epithelium to a mesenchyme phenotype is closely associated with organ fibrosis.[26] AEC2s act as a potential source of myofibroblasts during hyperoxia-induced EMT in lung tissue.[8] Cells that lose their epithelial phenotype become poorly attached to surrounding cells due to the loss of E-cadherin and abandon apical to basal polarity. To promote wound healing, epithelial features are replaced by enhanced expression of N-cadherin and Vimentin, which facilitate cell migration. In our study, reduced E-cadherin expression and increased N-cadherin and Vimentin expression indicated hyperoxia-induced EMT. Selective ER-phagy is activated by delivering ER fragments to lysosomes for degradation and limiting stress-induced ER expansion, thereby promoting cell survival,[25] a process believed to play a key role in maintaining ER homeostasis. We found that overexpression of FAM134B attenuated hyperoxia-induced EMT, indicating that ER homeostasis was critically associated with EMT.

Many studies have described the pro-survival role played by the PI3K/AKT pathway following hyperoxia exposure[30,40,41] and commented on the regulatory role played by FAM134B in the AKT pathway in hepatocellular carcinoma cells.[42] Based on our bioinformatic analysis, we hypothesized that the protective effect exerted by overexpressed FAM134B on hyperoxia-exposed cells may be achieved via the PI3K/AKT pathway. Experimental data indicated that the PI3K/AKT pathway was significantly inhibited following hyperoxia exposure, whereas overexpression of FAM134B activated the PI3K/AKT pathway. Next, we investigated the association between the PI3K/AKT pathway and the protective effects exerted by FAM134B on hyperoxia-exposed cells and rat lung tissue. The results showed that the PI3K/AKT pathway inhibitor, LY294002, reversed the protective effects exerted by FAM134B against hyperoxia exposure, as evidenced by increased apoptosis, decreased cell proliferation, increased EMT, and aggravated lung injury. These findings revealed that the PI3K/AKT pathway was associated with the protective effect exerted by FAM134B against hyperoxia exposure.

The beneficial ROS scavenging ability of $CeO_2$-NPs has been demonstrated in a variety of maladies, including limb ischemia,[43] acute kidney injury,[44] and hepatic ischemia-reperfusion injury.[22] $CeO_2$-NPs can also scavenge excess intracellular ROS generated during the inflammatory response.[45] Hyperoxia-induced lung injury is closely associated with excessive ROS production.[46] The results of the present study confirmed the scavenging effects exerted by $CeO_2$-NPs on excess ROS in hyperoxia-exposed RLE-6TN. Removal of excess ROS significantly

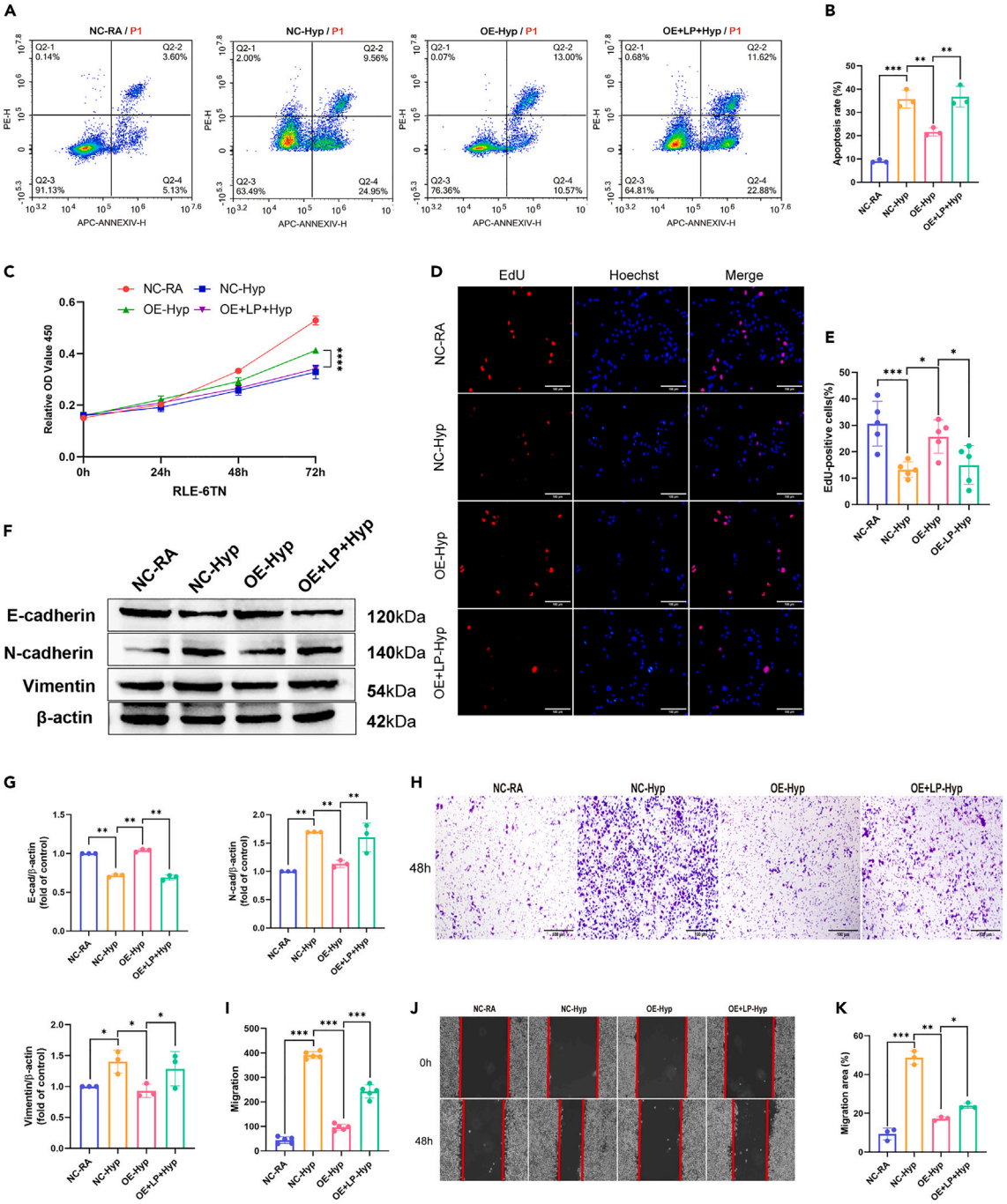


**Figure 4. Inhibition of the PI3K/AKT pathway by LY294002 reversed increased cell viability, and reduced apoptosis and EMT inhibition in RLE-6TN cells overexpressing FAM134B**

(A) Flow cytometry determination of apoptosis in each group.

(B) Quantitative analysis of flow cytometry results (±SD, $n = 3$).

(C–E) CCK8 (C, ±SD, $n = 3$) and EdU (D–E, ±SD, $n = 5$, scale bar:100 μm ) assay results of the effect of LY294002 on cell proliferation following overexpression of FAM134B.

(F) Western blot analysis of E-cadherin, N-cadherin, and Vimentin.

(G) Optical density analysis of E-cadherin, N-cadherin, and Vimentin (±SD, $n = 3$).

(H) RLE-6TN cells were visualized using phase-contrast microscopy for the analysis of migration ability (100× magnification; scale bar: 100 μm).

(I) Quantification of migrating cells was performed in transwell chambers (±SD, $n = 5$).

(J and K) A 48-h incubation period for RLE-6TN cells was followed by a wound-healing test (±SD, $n = 3$). RA: room air group; Hyp: hyperoxia group; NC: empty vector group; OE: FAM134B overexpression group; LP: LY294002 group; *$p < 0.05$, **$p < 0.01$, ***$p < 0.001$, ****$p < 0.0001$.

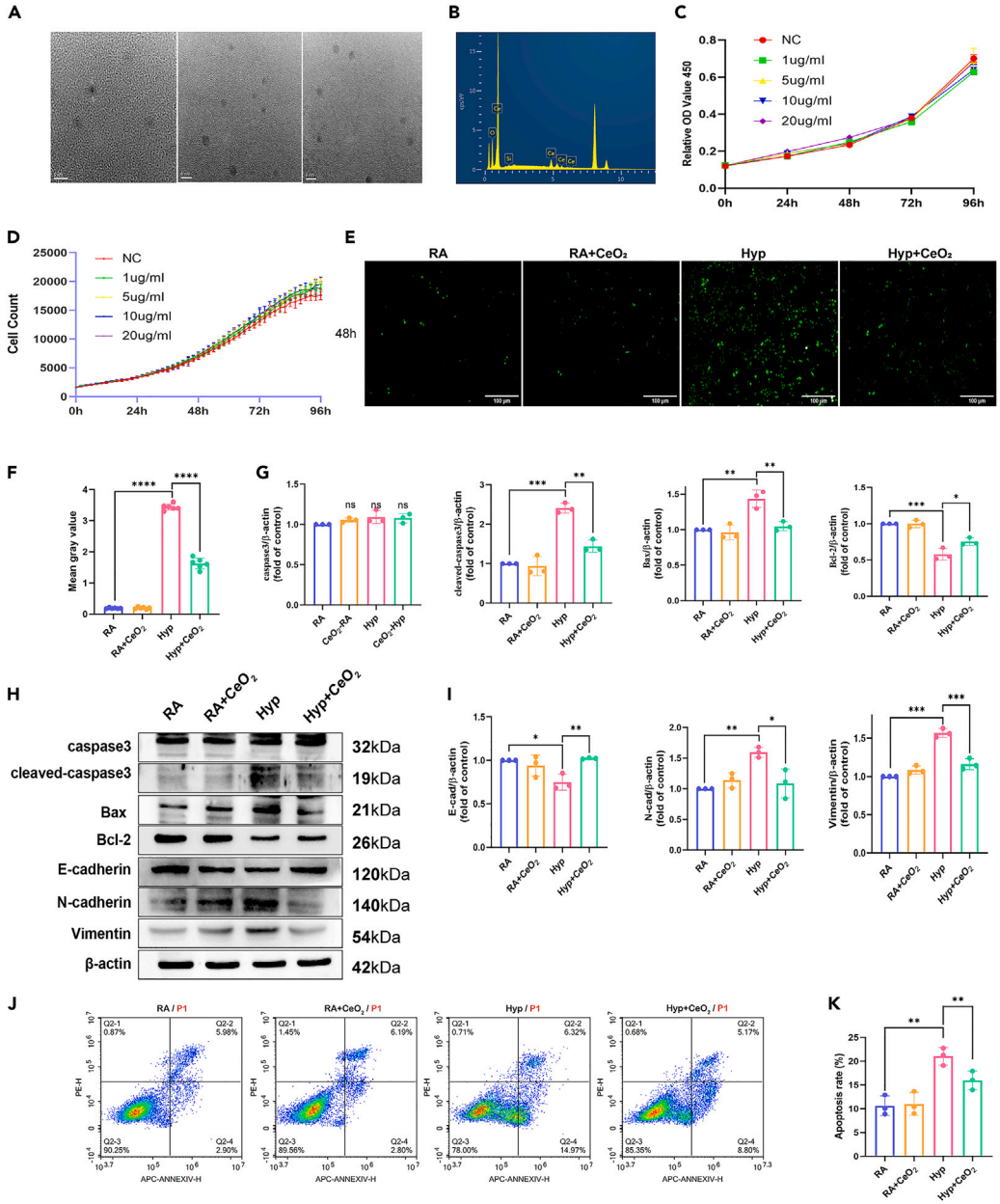


**Figure 5. $CeO_2$-NPs reduced apoptosis, decreased EMT, and increased the cell viability of AEC2s cells following hyperoxia exposure**

(A) Transmission electron microscopy image of $CeO_2$-NPs; scale bar inset: 5 nm.

(B) The energy-dispersive X-ray (EDX) spectrum of $CeO_2$-NPs demonstrated the presence of all essential chemical elements (Ce and O).

(C) CCK8 assessment of the cell growth with $CeO_2$-NPs (±SD, $n = 3$).

(D) Live cell imaging to assess cell growth with $CeO_2$-NPs (±SD, $n = 6$).

(E) The DCFH-DA probe detected the scavenging ability of $CeO_2$-NPs on reactive oxygen species (ROS) following hyperoxia exposure (100× magnification; scale bar: 100 μm).

(F) Mean grayscale values of the DCFH-DA probe used to detect the scavenging ability of $CeO_2$-NPs on ROS following hyperoxia exposure (±SD, $n = 5$).

(G) Optical density analysis of caspase3, cleaved-caspase3, Bax, and Bcl-2 (±SD, $n = 3$).

(H) Western blot analysis of the effect of $CeO_2$-NPs on the expression of caspase3, cleaved-caspase3, Bax, Bcl-2, E-cadherin, N-cadherin, and Vimentin in hyperoxia-exposed RLE-6TN cells.

(I) Optical density analysis of E-cadherin, N-cadherin, and Vimentin (±SD, $n = 3$).

(J) Flow cytometry determination of apoptosis in each group.

(K) Quantitative analysis of flow cytometry (±SD, $n = 3$). RA: room air group; Hyp: hyperoxia group; NC: control cell group; $CeO_2$: $CeO_2$-NPs group; $^*p < 0.05$, $^{**}p < 0.01$,$^{****}p < 0.0001$.

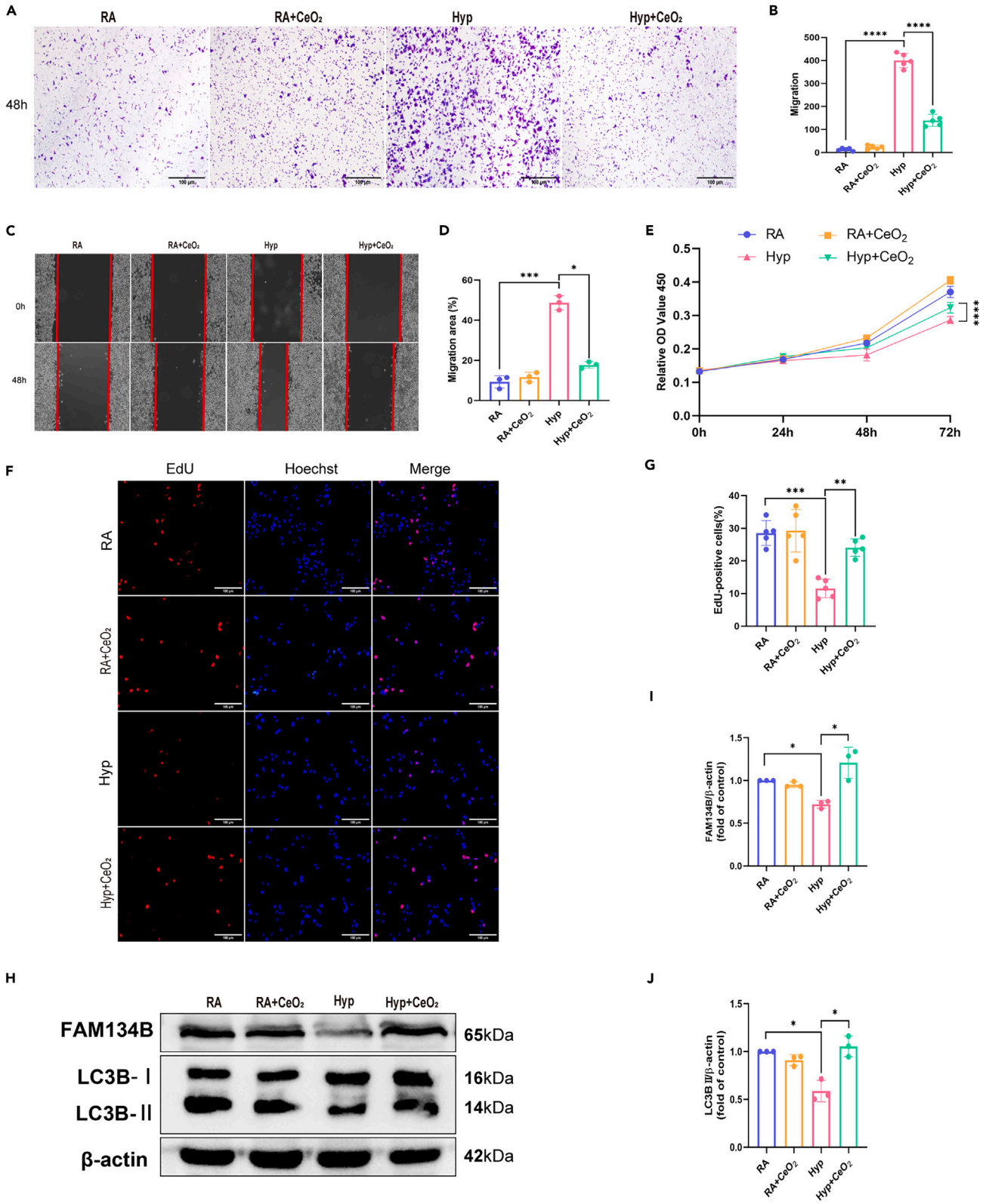
A
RA
RA+CeO2
Hyp
Hyp+CeO2
48h
B
Migration
C
0h
48h
D
Migration area (%)
E
Relative OD Value 450
0h
24h
48h
72h
F
EdU
Hoechst
Merge
G
EdU-positive cells(%)
I
FAM134B/β-actin (fold of control)
H
FAM134B
LC3B- Ⅰ
LC3B-Ⅱ
β-actin
65kDa
16kDa
14kDa
42kDa
J
LC3B Ⅱ/β-actin (fold of control)

**Figure 6. $CeO_2$-NPs decreased EMT, and increased the cell viability of AEC2s cells following hyperoxia exposure, thereby protecting against the impairment of ER-phagy levels following hyperoxia exposure**

(A) RLE-6TN cells were visualized using phase-contrast microscopy to analyze their migration ability (100× magnification; scale bar: 100 μm).

(B) Quantification of migrating cells was performed in Transwell chambers (±SD, $n = 5$).

(C and D) A 48-h incubation period for RLE-6TN cells was followed by a wound-healing test (±SD, $n = 3$).

(E–G) CCK8 (E, ±SD, $n = 3$) and EdU (F-G, ±SD, $n = 5$, scale bar: 100 μm) assay results of the effect of $CeO_2$-NPs on cell viability after hyperoxia exposure.

(H) Western blot analysis of FAM134B and LC3B.

(I) Optical density analysis of FAM134B (±SD, $n = 3$).

(J) Optical density analysis of LC3B (±SD, $n = 3$). RA: room air group; Hyp: hyperoxia group; $CeO_2$: $CeO_2$-NPs group; *$p < 0.05$, **$p < 0.01$, ***$p < 0.001$, ****$p < 0.0001$.

reduced apoptosis, promoted cellularity, and decreased EMT levels in hyperoxia-exposed RLE-6TN cells. $CeO_2$-NPs showed significant protective effects against lung damage in rats exposed to hyperoxia.

Our study confirmed that preventing ER-phagy from being impaired during hyperoxia may activate the PI3K/AKT pathway, thereby protecting against HALI. Thus, $CeO_2$-NPs may protect hyperoxia-exposed HALI by protecting ER-phagy. Further, we found that $CeO_2$-NPs intervention did not significantly downregulate FAM134B and inhibited the downregulation of LC3B in hyperoxia-exposed RLE-6N cells and rat lung tissue. This finding suggested that $CeO_2$-NPs may exert a protective effect on HALI by protecting ER-phagy.

Overall, our study suggests new mechanisms and protective strategies for HALI. Downregulation of the ER-phagy receptor, FAM134B, is a key factor in HALI. FAM134B protects AEC2s and rat lung tissues exposed to hyperoxia through activation of the PI3K/AKT pathway. $CeO_2$-NPs prevent downregulation of FAM134B and LC3B and attenuates HALI by scavenging excess ROS after hyperoxia exposure to maintain adequate levels of ER-phagy.

## Conclusions

Our data suggest that ER-phagy is inhibited by hyperoxia-induced injury and that maintaining ER autophagic activity is an effective strategy that protects against HALI. To the best of our knowledge, the current study is the first to report that FAM134B is involved in HALI and hyperoxia-induced apoptosis, proliferation, and EMT of AEC2s and demonstrate that the modulatory effect exerted by FAM134B on the PI3K/AKT signaling pathway confers a protective effect against hyperoxia-induced injury. Furthermore, this study is also the first to report the protective effects exerted by $CeO_2$-NPS against HALI and clarify the underlying mechanisms involving attenuation of the downregulation of FAM134B. Thus, the activation of FAM134B-mediated ER-phagy may provide a potential therapeutic target in the prevention of HALI. $CeO_2$-NPs also exert a protective effect against hyperoxia-induced injury in AEC2s and lung tissue.

## Limitations of the study

First, this study did not explore whether FAM134B directly regulates the PI3K/AKT signaling pathway; and the issue of the time course of changes in injury endpoints in control or lentiviral protected rats may be very important and is not addressed, in addition; this study did not localize the nanoparticles in lung tissues and cells. Finally, Our data were generated using male rats starting at 6–7 weeks of age and used an $O_2$ concentration of 90 ± 2% for 7 days; hence, results may be different when using younger or older male rats at higher or lower hyperoxia exposure for a different duration. These elements also need to be further investigated in the future.

## STAR★METHODS

Detailed methods are provided in the online version of this paper and include the following:

- KEY RESOURCES TABLE
- RESOURCE AVAILABILITY
  - Lead contact
  - Materials availability
  - Data and code availability
- EXPERIMENTAL MODEL AND STUDY PARTICIPANT DETAILS
  - Cell culture and processing
  - Animal experiments
  - Animal treatment
  - Hyperoxia-induced lung injury model
  - Experiment 1
  - Experiment 2
- METHOD DETAILS
  - Western blotting
  - CCK-8 and EdU assays
  - Wound-healing assay and transwell migration
  - Live-cell imaging and transmission electron microscopy

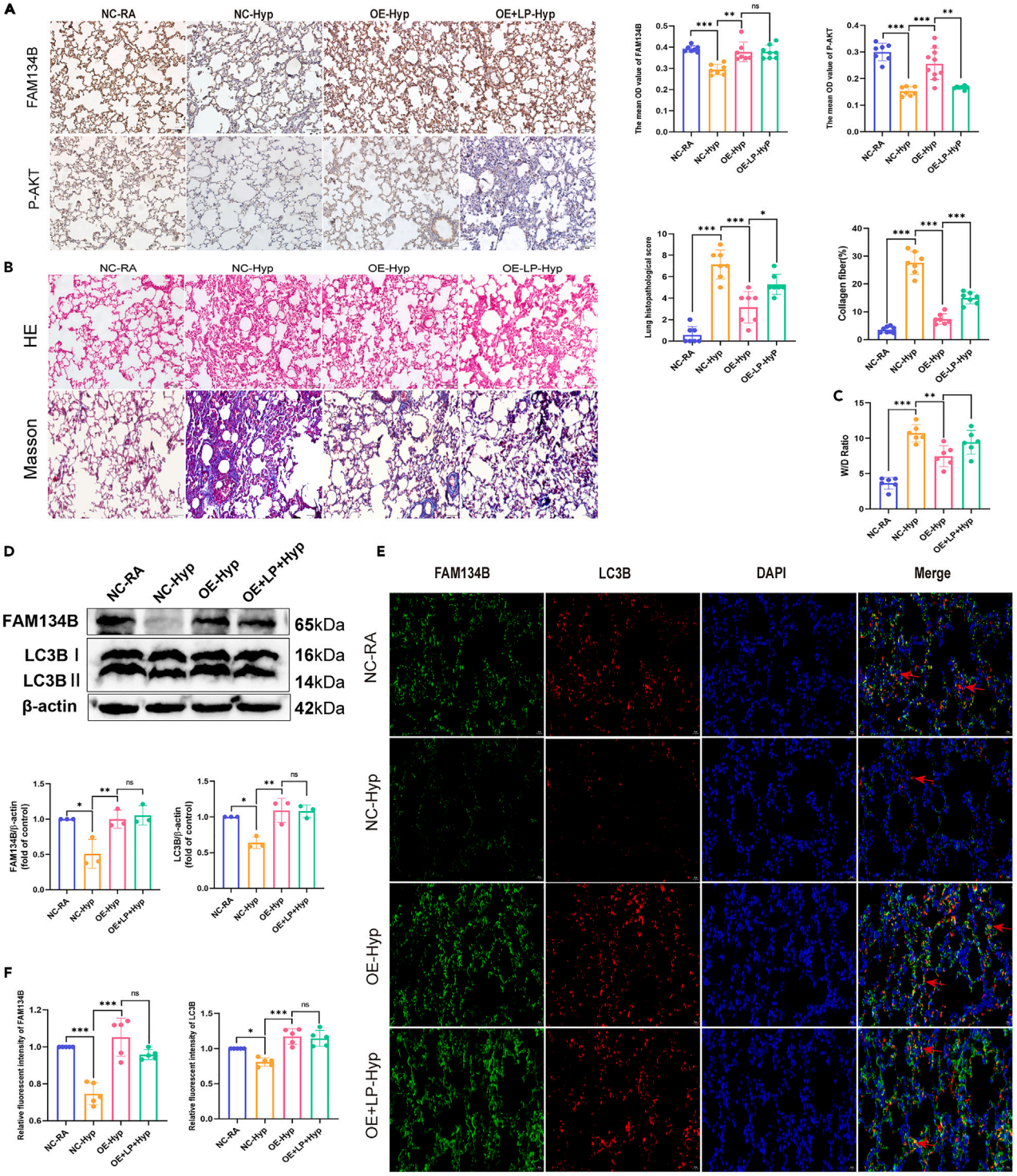


**Figure 7. Overexpression of FAM134B in SD rat lung tissues activates P-AKT and attenuates HALI, whereas LY294002 reverses these effects**

(A) Immunohistochemical staining of FAM134B and P-AKT in lung tissues of different treatment groups, scale bar; 100 μm, magnification 200 ×, ±SD, $n = 7$.

(B) H&E staining and Masson staining. Scale bar; 100 μm, magnification 200 ×, ±SD, $n = 7$.

(C) Effect of different groups on lung wet/dry (W/D) ratio, ±SD, $n = 6$.

(D) Western blot analysis of FAM134B, and LC3B, ±SD, $n = 3$.

(E and F) Immunofluorescence staining of FAM134B and LC3B in lung tissues. Scale bar; 50 μm, magnification 400 ×, ±SD, $n = 5$. RA: room air group; NC: empty vector group; Hyp: hyperoxia group; OE: FAM134B overexpression group; LP: LY294002 group. *$p < 0.05$, **$p < 0.01$, ***$p < 0.001$, ****$p < 0.0001$.

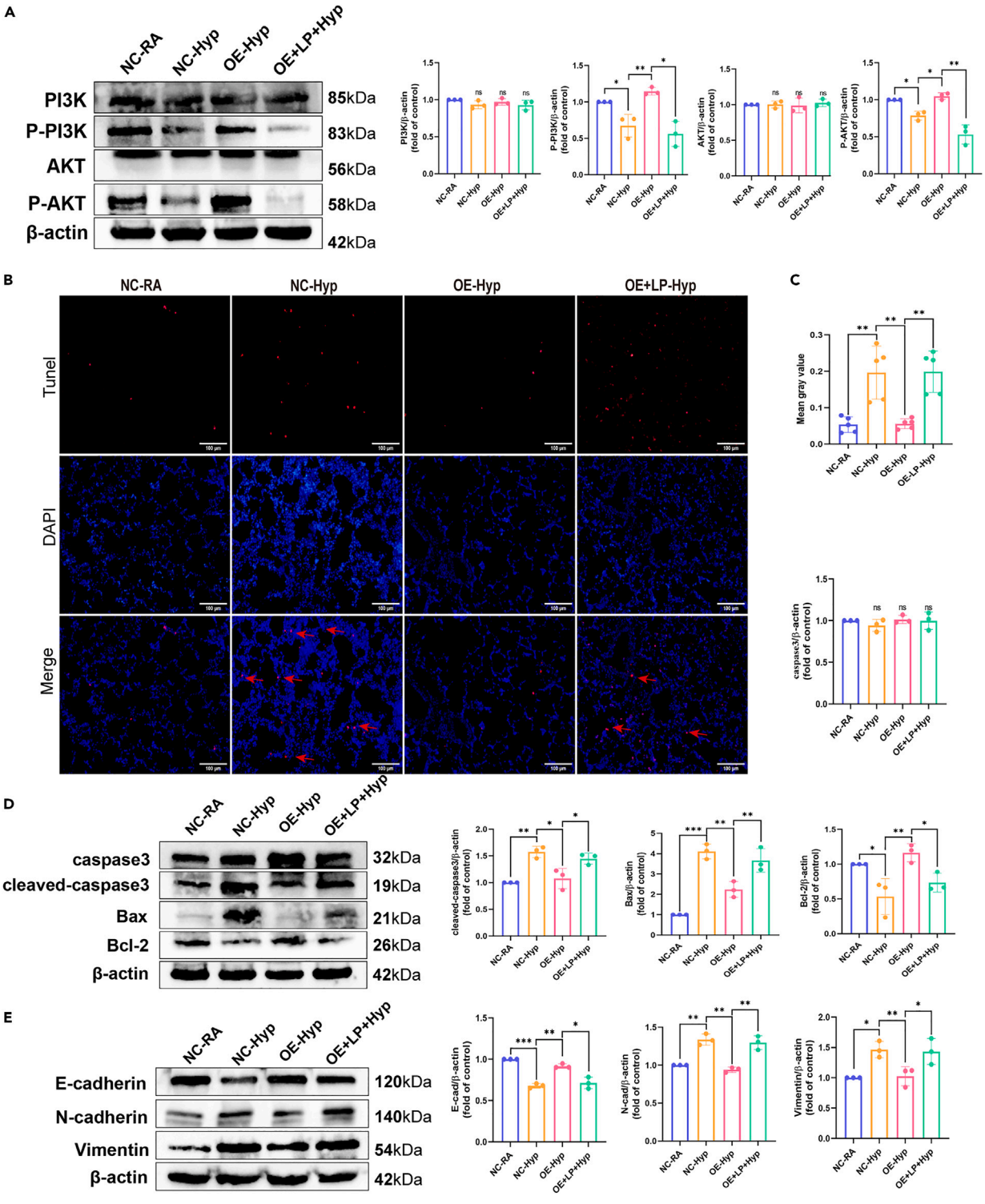


**Figure 8. Overexpression of FAM134B in SD rat lung tissues activates P-AKT and attenuates HALI, whereas LY294002 reverses these effects**

(A) Western blot analysis of PI3K, P-PI3K, AKT, P-AKT in rat lung following overexpression of FAM134B, ±SD, $n = 3$.

(B and C) TUNEL images of lung tissue from rat in different groups, scale bar; 100 μm, magnification 200 ×, ±SD, $n = 5$.

(D) Western blot analysis of caspase3, cleaved-caspase3, Bax, and Bcl-2 in rat lung (±SD, $n = 3$).

(E) Western blot analysis of E-cadherin, N-cadherin, and Vimentin in rat lung (±SD, $n = 3$). RA: room air group; NC: empty vector group; Hyp: hyperoxia group; OE: FAM134B overexpression group; LP: LY294002 group. *$p < 0.05$, **$p < 0.01$, ***$p < 0.001$, ****$p < 0.0001$.

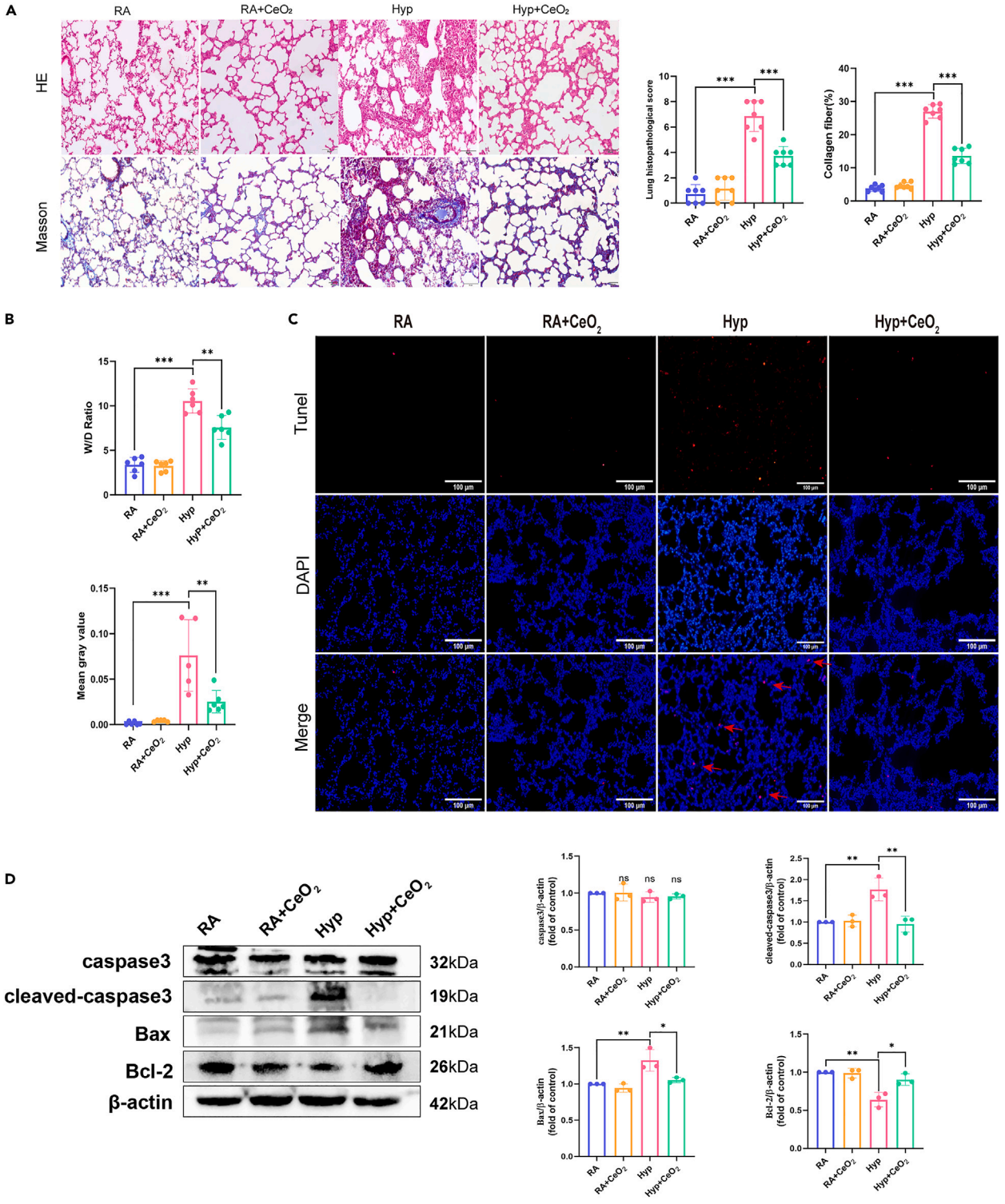


**Figure 9. $CeO_2$-NPs attenuates lung injury in SD rats**

(A) H&E staining and Masson staining after $CeO_2$-NPs treatment. Scale bar; 100 μm, magnification 200 ×, ±SD, $n = 7$.

(B) Effect of different groups on lung wet/dry (W/D) ratio (±SD, $n = 6$).

(C) TUNEL images of lung tissue from rat after $CeO_2$-NPs treatment, scale bar; 100 μm, magnification 200 ×, (±SD, $n = 5$).

(D) Western blot analysis of caspase3, cleaved-caspase3, Bax, and Bcl-2 in rat lung (±SD, $n = 3$). RA: room air group; Hyp: hyperoxia group; $CeO_2$: $CeO_2$-NPs group. *$p < 0.05$, **$p < 0.01$, ***$p < 0.001$, ****$p < 0.0001$.

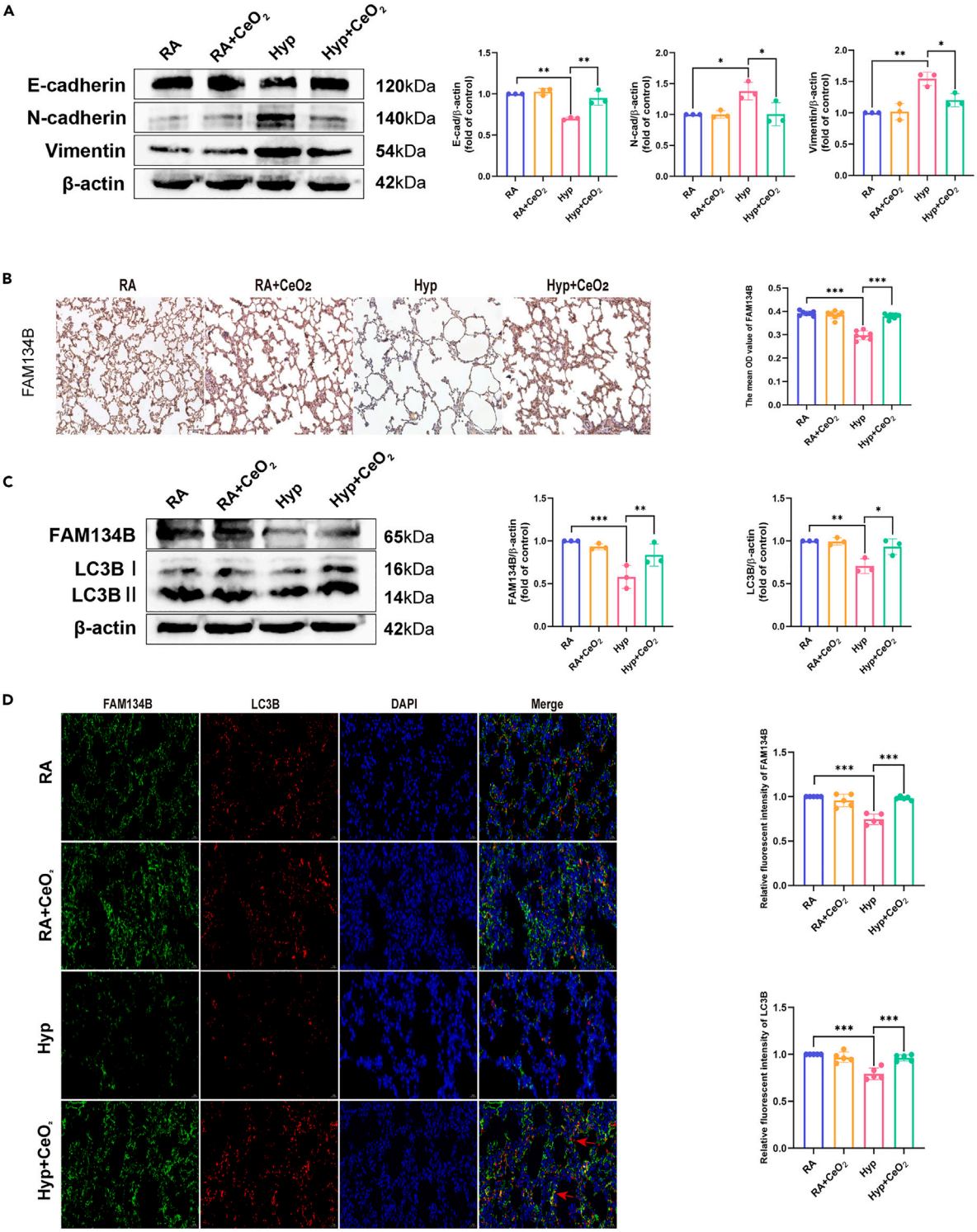


**Figure 10. $CeO_2$-NPs attenuates lung injury and inhibits hyperoxia-induced downregulation of FAM134B in SD rats**

(A) Western blot analysis of E-cadherin, N-cadherin, and Vimentin in rat lung after $CeO_2$-NPs treatment (±SD, $n = 3$).

(B) Immunofluorescence staining of FAM134B in lung tissues. Scale bar; 50 μm, magnification 200 ×, ±SD, $n = 7$.

(C) Western blot analysis of FAM134B, and LC3B (±SD, $n = 3$).

(D) Immunofluorescence staining of FAM134B and LC3B in lung tissues after $CeO_2$-NPs treatment. Scale bar; 50 μm, magnification 400 ×, ±SD, $n = 5$. RA: room air group; Hyp: hyperoxia group; $CeO_2$-NPs group. *$p < 0.05$, **$p < 0.01$, ***$p < 0.001$, ****$p < 0.0001$.

- Detection of ROS production
- Real-time fluorescence qPCR
- Flow cytometry
- Wet/dry lung weight ratio
- Histopathology of lung tissue
- Immunohistochemistry and immunofluorescence
- Masson trichrome staining
- TUNEL staining

- QUANTIFICATION AND STATISTICAL ANALYSIS

## ACKNOWLEDGMENTS

This work was supported by the Natural Science Foundation of Gansu Province (21JR1RA062).

## AUTHOR CONTRIBUTIONS

H.G.: designed the research and conducted the most of the experiments. R.-R. H.: collated data, data curation. S.-S.Q.: collated data, data curation. Y.Y.: assisted experiments. S.-H.C.: assisted experiments. S.-L.D.: assisted experiments. Y.-L.L.: coordinated and directed the project.

## DECLARATION OF INTERESTS

The authors declare no competing financial interests.

Received: September 6, 2023
Revised: November 21, 2023
Accepted: June 24, 2024
Published: June 26, 2024

## REFERENCES

1. Chu, D.K., Kim, L.H.Y., Young, P.J., Zamiri, N., Almenawer, S.A., Jaeschke, R., Szczeklik, W., Schünemann, H.J., Neary, J.D., and Alhazzani, W. (2018). Mortality and morbidity in acutely ill adults treated with liberal versus conservative oxygen therapy (IOTA): a systematic review and meta-analysis. Lancet *391*, 1693–1705. https://doi.org/10.1016/S0140-6736(18)30479-3.
2. Girardis, M., Busani, S., Damiani, E., Donati, A., Rinaldi, L., Marudi, A., Morelli, A., Antonelli, M., and Singer, M. (2016). Effect of Conservative vs Conventional Oxygen Therapy on Mortality Among Patients in an Intensive Care Unit: The Oxygen-ICU Randomized Clinical Trial. JAMA *316*, 1583–1589. https://doi.org/10.1001/jama.2016.11993.
3. Sureshbabu, A., Syed, M., Das, P., Janér, C., Pryhuber, G., Rahman, A., Andersson, S., Homer, R.J., and Bhandari, V. (2016). Inhibition of Regulatory-Associated Protein of Mechanistic Target of Rapamycin Prevents Hyperoxia-Induced Lung Injury by Enhancing Autophagy and Reducing Apoptosis in Neonatal Mice. Am. J. Respir. Cell Mol. Biol. *55*, 722–735. https://doi.org/10.1165/rcmb.2015-0349OC.
4. Kallet, R.H., and Matthay, M.A. (2013). Hyperoxic acute lung injury. Respir. Care *58*, 123–141. https://doi.org/10.4187/respcare.01963.
5. Bhandari, V., Choo-Wing, R., Lee, C.G., Zhu, Z., Nedrelow, J.H., Chupp, G.L., Zhang, X., Matthay, M.A., Ware, L.B., Homer, R.J., et al. (2006). Hyperoxia causes angiopoietin 2-mediated acute lung injury and necrotic cell death. Nat. Med. *12*, 1286–1293. https://doi.org/10.1038/nm1494.
6. Thomson, S., Petti, F., Sujka-Kwok, I., Mercado, P., Bean, J., Monaghan, M., Seymour, S.L., Argast, G.M., Epstein, D.M., and Haley, J.D. (2011). A systems view of epithelial-mesenchymal transition signaling states. Clin. Exp. Metastasis *28*, 137–155. https://doi.org/10.1007/s10585-010-9367-3.
7. Zhang, L., Zhao, S., Yuan, L., Wu, H., Jiang, H., and Luo, G. (2016). Placenta growth factor contributes to cell apoptosis and epithelial-to-mesenchymal transition in the hyperoxia-induced acute lung injury. Life Sci. *156*, 30–37. https://doi.org/10.1016/j.lfs.2016.05.024.
8. Vyas-Read, S., Wang, W., Kato, S., Colvocoresses-Dodds, J., Fifadara, N.H., Gauthier, T.W., Helms, M.N., Carlton, D.P., and Brown, L.A.S. (2014). Hyperoxia induces alveolar epithelial-to-mesenchymal cell transition. Am. J. Physiol. Lung Cell Mol. Physiol. *306*, L326–L340. https://doi.org/10.1152/ajplung.00074.2013.
9. Xia, S., Vila Ellis, L., Winkley, K., Menden, H., Mabry, S.M., Venkatraman, A., Louiselle, D., Gibson, M., Grundberg, E., Chen, J., and Sampath, V. (2023). Neonatal hyperoxia induces activated pulmonary cellular states and sex-dependent transcriptomic changes in a model of experimental bronchopulmonary dysplasia. Am. J. Physiol. Lung Cell Mol. Physiol. *324*, L123–L140. https://doi.org/10.1152/ajplung.00252.2022.
10. Budinger, G.R.S., Mutlu, G.M., Urich, D., Soberanes, S., Buccellato, L.J., Hawkins, K., Chiarella, S.E., Radigan, K.A., Eisenbart, J., Agrawal, H., et al. (2011). Epithelial cell death is an important contributor to oxidant-mediated acute lung injury. Am. J. Respir. Crit. Care Med. *183*, 1043–1054. https://doi.org/10.1164/rccm.201002-0181OC.
11. Friedman, J.R., and Voeltz, G.K. (2011). The ER in 3D: a multifunctional dynamic membrane network. Trends Cell Biol. *21*, 709–717. https://doi.org/10.1016/j.tcb.2011.07.004.
12. Pao, H.-P., Liao, W.-I., Tang, S.-E., Wu, S.-Y., Huang, K.-L., and Chu, S.-J. (2021). Suppression of Endoplasmic Reticulum Stress by 4-PBA Protects Against Hyperoxia-Induced Acute Lung Injury via Up-Regulating Claudin-4 Expression. Front. Immunol. *12*, 674316. https://doi.org/10.3389/fimmu.2021.674316.
13. Yao, M., Pu, P.-M., Li, Z.-Y., Zhu, K., Zhou, L.-Y., Sun, Y.-L., Dai, Y.-X., Cui, X.-J., and Wang, Y.-J. (2023). Melatonin restores endoplasmic reticulum homeostasis to protect injured neurons in a rat model of chronic cervical cord compression. J. Pineal Res. *74*, e12859. https://doi.org/10.1111/jpi.12859.
14. Chen, W., Mao, H., Chen, L., and Li, L. (2022). The pivotal role of FAM134B in selective ER-phagy and diseases. Biochim. Biophys. Acta. Mol. Cell Res. *1869*, 119277. https://doi.org/10.1016/j.bbamcr.2022.119277.
15. Bhaskara, R.M., Grumati, P., Garcia-Pardo, J., Kalayil, S., Covarrubias-Pinto, A., Chen, W., Kudryashev, M., Dikic, I., and Hummer, G. (2019). Curvature induction and membrane remodeling by FAM134B reticulon homology domain assist selective ER-phagy. Nat. Commun. *10*, 2370. https://doi.org/10.1038/s41467-019-10345-3.
16. Luo, R., Li, S., Li, G., Lu, S., Zhang, W., Liu, H., Lei, J., Ma, L., Ke, W., Liao, Z., et al. (2021). FAM134B-Mediated ER-phagy Upregulation Attenuates AGEs-Induced Apoptosis and Senescence in Human Nucleus Pulposus

Cells. Oxid. Med. Cell. Longev. *2021*, 3843145. https://doi.org/10.1155/2021/3843145.
17. Xie, N., Li, Y., Wang, C., Lian, Y., Zhang, H., Li, Y., Meng, X., and Du, L. (2020). FAM134B Attenuates Seizure-Induced Apoptosis and Endoplasmic Reticulum Stress in Hippocampal Neurons by Promoting Autophagy. Cell. Mol. Neurobiol. *40*, 1297–1305. https://doi.org/10.1007/s10571-020-00814-5.
18. Chipurupalli, S., Ganesan, R., Martini, G., Mele, L., Reggio, A., Esposito, M., Kannan, E., Namasivayam, V., Grumati, P., Desiderio, V., and Robinson, N. (2022). Cancer cells adapt FAM134B/BiP mediated ER-phagy to survive hypoxic stress. Cell Death Dis. *13*, 357. https://doi.org/10.1038/s41419-022-04813-w.
19. Li, H., Xia, P., Pan, S., Qi, Z., Fu, C., Yu, Z., Kong, W., Chang, Y., Wang, K., Wu, D., and Yang, X. (2020). The Advances of Ceria Nanoparticles for Biomedical Applications in Orthopaedics. Int. J. Nanomedicine *15*, 7199–7214. https://doi.org/10.2147/IJN.S270229.
20. Lord, M.S., Berret, J.F., Singh, S., Vinu, A., and Karakoti, A.S. (2021). Redox Active Cerium Oxide Nanoparticles: Current Status and Burning Issues. Small *17*, e2102342. https://doi.org/10.1002/smll.202102342.
21. Korsvik, C., Patil, S., Seal, S., and Self, W.T. (2007). Superoxide dismutase mimetic properties exhibited by vacancy engineered ceria nanoparticles. Chem. Commun. *10*, 1056–1058. https://doi.org/10.1039/b615134e.
22. Ni, D., Wei, H., Chen, W., Bao, Q., Rosenkrans, Z.T., Barnhart, T.E., Ferreira, C.A., Wang, Y., Yao, H., Sun, T., et al. (2019). Ceria Nanoparticles Meet Hepatic Ischemia-Reperfusion Injury: The Perfect Imperfection. Adv. Mater. *31*, e1902956. https://doi.org/10.1002/adma.201902956.
23. Oró, D., Yudina, T., Fernández-Varo, G., Casals, E., Reichenbach, V., Casals, G., González de la Presa, B., Sandalinas, S., Carvajal, S., Puntes, V., and Jiménez, W. (2016). Cerium oxide nanoparticles reduce steatosis, portal hypertension and display anti-inflammatory properties in rats with liver fibrosis. J. Hepatol. *64*, 691–698. https://doi.org/10.1016/j.jhep.2015.10.020.
24. Yao, C., Wang, W., Wang, P., Zhao, M., Li, X., and Zhang, F. (2018). Near-Infrared Upconversion Mesoporous Cerium Oxide Hollow Biophotocatalyst for Concurrent pH-/H2 O2 -Responsive O2 -Evolving Synergetic Cancer Therapy. Adv. Mater. *30*, 1704833. https://doi.org/10.1002/adma.201704833.
25. Vargas, J.N.S., Hamasaki, M., Kawabata, T., Youle, R.J., and Yoshimori, T. (2023). The mechanisms and roles of selective autophagy in mammals. Nat. Rev. Mol. Cell Biol. *24*, 167–185. https://doi.org/10.1038/s41580-022-00542-2.
26. Kalluri, R., and Weinberg, R.A. (2009). The basics of epithelial-mesenchymal transition. J. Clin. Invest. *119*, 1420–1428. https://doi.org/10.1172/JCI39104.
27. Jung, J., Yang, K., Kim, H.-J., Lee, Y.-J., Kim, M., Choi, Y.-H., and Kang, J.L. (2019). RhoA-Dependent HGF and c-Met Mediate Gas6-Induced Inhibition of Epithelial-Mesenchymal Transition, Migration, and Invasion of Lung Alveolar Epithelial Cells. Biomolecules *9*, 565. https://doi.org/10.3390/biom9100565.
28. Whiteman, E.L., Cho, H., and Birnbaum, M.J. (2002). Role of Akt/protein kinase B in metabolism. Trends Endocrinol. Metab. *13*, 444–451. https://doi.org/10.1016/s1043-2760(02)00662-8.
29. Plas, D.R., and Thompson, C.B. (2002). Cell metabolism in the regulation of programmed cell death. Trends Endocrinol. Metab. *13*, 75–78. https://doi.org/10.1016/s1043-2760(01)00528-8.
30. Alphonse, R.S., Vadivel, A., Coltan, L., Eaton, F., Barr, A.J., Dyck, J.R.B., and Thébaud, B. (2011). Activation of Akt protects alveoli from neonatal oxygen-induced lung injury. Am. J. Respir. Cell Mol. Biol. *44*, 146–154. https://doi.org/10.1165/rcmb.2009-0182OC.
31. Patel, A., Kosanovich, J., Sansare, S., Balmuri, S., Sant, V., Empey, K.M., and Sant, S. (2023). In vitro and in vivo evaluation of cerium oxide nanoparticles in respiratory syncytial virus infection. Bioact. Mater. *24*, 124–135. https://doi.org/10.1016/j.bioactmat.2022.12.005.
32. Wang, X.-X., Sha, X.-L., Li, Y.-L., Li, C.-L., Chen, S.-H., Wang, J.-J., and Xia, Z. (2020). Lung injury induced by short-term mechanical ventilation with hyperoxia and its mitigation by deferoxamine in rats. BMC Anesthesiol. *20*, 188. https://doi.org/10.1186/s12871-020-01089-5.
33. Das, G., Shravage, B.V., and Baehrecke, E.H. (2012). Regulation and function of autophagy during cell survival and cell death. Cold Spring Harb. Perspect. Biol. *4*, a008813. https://doi.org/10.1101/cshperspect.a008813.
34. Bravo-San Pedro, J.M., Kroemer, G., and Galluzzi, L. (2017). Autophagy and Mitophagy in Cardiovascular Disease. Circ. Res. *120*, 1812–1824. https://doi.org/10.1161/CIRCRESAHA.117.311082.
35. Reggiori, F., and Molinari, M. (2022). ER-phagy: mechanisms, regulation, and diseases connected to the lysosomal clearance of the endoplasmic reticulum. Physiol. Rev. *102*, 1393–1448. https://doi.org/10.1152/physrev.00038.2021.
36. Kurth, I., Pamminger, T., Hennings, J.C., Soehendra, D., Huebner, A.K., Rotthier, A., Baets, J., Senderek, J., Topaloglu, H., Farrell, S.A., et al. (2009). Mutations in FAM134B, encoding a newly identified Golgi protein, cause severe sensory and autonomic neuropathy. Nat. Genet. *41*, 1179–1181. https://doi.org/10.1038/ng.464.
37. Khaminets, A., Heinrich, T., Mari, M., Grumati, P., Huebner, A.K., Akutsu, M., Liebmann, L., Stolz, A., Nietzsche, S., Koch, N., et al. (2015). Regulation of endoplasmic reticulum turnover by selective autophagy. Nature *522*, 354–358. https://doi.org/10.1038/nature14498.
38. Qu, Y., Gao, R., Wei, X., Sun, X., Yang, K., Shi, H., Gao, Y., Hu, S., Wang, Y., Yang, J., et al. (2022). Gasdermin D mediates endoplasmic reticulum stress via FAM134B to regulate cardiomyocyte autophagy and apoptosis in doxorubicin-induced cardiotoxicity. Cell Death Dis. *13*, 901. https://doi.org/10.1038/s41419-022-05333-3.
39. Zhang, D., Zhao, X., Zhang, D., Gao, S., Xue, X., and Fu, J. (2020). Hyperoxia reduces STX17 expression and inhibits the autophagic flux in alveolar type II epithelial cells in newborn rats. Int. J. Mol. Med. *46*, 773–781. https://doi.org/10.3892/ijmm.2020.4617.
40. Truong, S.V., Monick, M.M., Yarovinsky, T.O., Powers, L.S., Nyunoya, T., and Hunninghake, G.W. (2004). Extracellular signal-regulated kinase activation delays hyperoxia-induced epithelial cell death in conditions of Akt downregulation. Am. J. Respir. Cell Mol. Biol. *31*, 611–618. https://doi.org/10.1165/rcmb.2004-0141OC.
41. Wu, D., Liang, M., Dang, H., Fang, F., Xu, F., and Liu, C. (2018). Hydrogen protects against hyperoxia-induced apoptosis in type II alveolar epithelial cells via activation of PI3K/Akt/Foxo3a signaling pathway. Biochem. Biophys. Res. Commun. *495*, 1620–1627. https://doi.org/10.1016/j.bbrc.2017.11.193.
42. Zhang, Z.-Q., Chen, J., Huang, W.-Q., Ning, D., Liu, Q.-M., Wang, C., Zhang, L., Ren, L., Chu, L., Liang, H.-F., et al. (2019). FAM134B induces tumorigenesis and epithelial-to-mesenchymal transition via Akt signaling in hepatocellular carcinoma. Mol. Oncol. *13*, 792–810. https://doi.org/10.1002/1878-0261.12429.
43. Park, I.-S., Mahapatra, C., Park, J.S., Dashnyam, K., Kim, J.-W., Ahn, J.C., Chung, P.-S., Yoon, D.S., Mandakhbayar, N., Singh, R.K., et al. (2020). Revascularization and limb salvage following critical limb ischemia by nanoceria-induced Ref-1/APE1-dependent angiogenesis. Biomaterials *242*, 119919. https://doi.org/10.1016/j.biomaterials.2020.119919.
44. Manne, N.D.P.K., Arvapalli, R., Nepal, N., Shokuhfar, T., Rice, K.M., Asano, S., and Blough, E.R. (2015). Cerium oxide nanoparticles attenuate acute kidney injury induced by intra-abdominal infection in Sprague-Dawley rats. J. Nanobiotechnology *13*, 75. https://doi.org/10.1186/s12951-015-0135-z.
45. Lord, M.S., Jung, M., Teoh, W.Y., Gunawan, C., Vassie, J.A., Amal, R., and Whitelock, J.M. (2012). Cellular uptake and reactive oxygen species modulation of cerium oxide nanoparticles in human monocyte cell line U937. Biomaterials *33*, 7915–7924. https://doi.org/10.1016/j.biomaterials.2012.07.024.
46. Singer, M., Young, P.J., Laffey, J.G., Asfar, P., Taccone, F.S., Skrifvars, M.B., Meyhoff, C.S., and Radermacher, P. (2021). Dangers of hyperoxia. Crit. Care *25*, 440. https://doi.org/10.1186/s13054-021-03815-y.

## STAR★METHODS

### KEY RESOURCES TABLE

| REAGENT or RESOURCE | SOURCE | IDENTIFIER |
|---|---|---|
| Antibodies | | |
| anti-FAM134B antibody | Proteintech | Cat# 21537-1-AP; RRID: AB_2878879 |
| anti-LC3B antibody | Abmart | Cat# T55992; RRID: AB_2929010 |
| anti-caspase3 antibody | Proteintech | Cat# 19677-1-AP; RRID: AB_10733244 |
| anti-Bax antibody | Abmart | Cat# T40051;RRID: AB_2910262 |
| anti-Bcl-2 antibody | Abmart | Cat# T40056;RRID: AB_2929011 |
| anti-E-cadherin antibody | Abmart | Cat# TA0131; RRID: AB_2936787 |
| anti-N-cadherin antibody | Abmart | Cat# T55015; RRID: AB_2937047 |
| anti-vimentin antibody | Abmart | Cat# T55134; RRID: AB_2938551 |
| anti-PI3K antibody | Abmart | Cat# T40115; RRID: AB_2936324 |
| anti-P-PI3K antibody | Abmart | Cat# T40065; RRID: AB_2936992 |
| anti-AKT antibody | Proteintech | Cat# 60203-2-Ig; RRID: AB_10912803 |
| anti-P-AKT antibody | Proteintech | Cat# 80455-1-RR; RRID: AB_2918892 |
| anti-Beta-actin antibody | Servicebio | Cat# GB15003; RRID: AB_3083699 |
| HRP-conjugated Affinipure Goat Anti-Mouse IgG | Proteintech | Cat# SA00001-1-A; RRID: AB_2890995 |
| HRP-conjugated Affinipure Goat Anti-Rabbit IgG | Proteintech | Cat# SA00001-2; RRID: AB_2722564 |
| Bacterial and virus strains | | |
| LV-Retreg1(FAM134B) | GeneChem (Shanghai, China). | GOSL0345088 |
| AAV-Retreg1(FAM134B) | GeneChem (Shanghai, China). | GOSV0358136 |
| Chemicals, peptides, and recombinant proteins | | |
| Cerium oxide nanoparticles | XFNANO | Cat#102847 |
| LY 294002 | GLPBIO | Cat#GC15485 |
| LY 294002 hydrochloride | GLPBIO | Cat#GC50009 |
| protease inhibitor | Boster | Cat#AR1178 |
| phosphatase inhibitor | Boster | Cat#AR1183 |
| Critical commercial assays | | |
| RIPA buffe | Boster | AR0102 |
| BCA Protein Assay Kit | Boster | AR1189 |
| ECL | Boster | AR1197 |
| Cell Counting Kit-8 | Beyotime | C0038 |
| Reactive Oxygen Species Assay Kit | Beyotime | C0071S |
| PrimeScript RT Reagent Kit | Beyotime | RR047A |
| Trizol reagent | Servicebio | G3013 |
| TB Green premix Ex Taq | Takara | RR820A |
| Annexin V-IF647/PI Cell Apoptosis Detection Kit | Servicebio | G1514 |
| Masson's Muscle Trichrome Staining Kit | Solarbio | G1340 |
| TMR (red) Tunel Cell Apoptosis Detection Kit | Servicebio | G1502 |
| Deposited data | | |
| Raw and analyzed data | This paper | GEO:GSE125489 |

(*Continued on next page*)

*Continued*

| REAGENT or RESOURCE | SOURCE | IDENTIFIER |
|---|---|---|
| Experimental models: Cell lines | | |
| rat alveolar type II epithelial cell line RLE-6TN | BeNa Culture Collection | BNCC337708 |
| Experimental models: Organisms/strains | | |
| About three-week-old male Sprague–Dawley (SD) rats | Lanzhou University | LDYYLL2022-216 |
| Software and algorithms | | |
| ImageJ software | Schneider et al., 2012 | https://imagej.nih.gov/ij |
| GraphPad Prism 9 | GraphPad Prism Software, Inc | https://www.graphpad.com/ |

## RESOURCE AVAILABILITY

### Lead contact

Further information and requests for resources and reagents should be directed to and will be fulfilled by the lead contact, Yu-Lan Li (liyul@lzu.edu.cn).

### Materials availability

This study did not generate new unique reagents and all materials in this study are commercially available.

### Data and code availability

- RNA-sequencing data was deposited at GEO and are publicly available as of the date of publication. Accession numbers are listed in the key resources table.
- This paper does not report original code.
- Any additional information required to reanalyze the data reported in this paper is available from the lead contact upon request.

## EXPERIMENTAL MODEL AND STUDY PARTICIPANT DETAILS

### Cell culture and processing

The rat alveolar type II epithelial cell line RLE-6TN (BNCC337708) was obtained from BeNa Culture Collection (Beijing, China). RLE-6TN was cultured in RPMI-1640 medium (C22400500BT, Gibco) containing 10% fetal bovine serum (AB-FBS-1050S, ABW) and 1% penicillin-streptomycin (03-031-1B, BI) and incubated at 37°C in an atmosphere of 5% $CO_2$ with 95% of either oxygen or room air (21% $O_2$) for hyperoxic or normoxic (control) cultures, respectively. For lentiviral transfection, FAM134B overexpressing lentivirus was designed and constructed by GeneChem (Shanghai, China). To inhibit the PI3K/AKT pathway, cells were treated with LY294002 (GC15485, GLPBIO) at 10 μM. Cerium oxide nanoparticles(1306-38-3, XFNANO) were used at 10 μg/mL.

### Animal experiments

About three-week-old male Sprague–Dawley (SD) rats were purchased from Lanzhou University (Lanzhou, China). All experiments were conducted in accordance with the Guidelines for Ethical Review of the National Laboratory Animal Welfare of the People's Republic of China (GB/T 35892-2018) and approved by the Animal Ethics Committee of the First Hospital of Lanzhou University (LDYYLL2022-216). The rats were humanely cared for throughout the experiment. The rats were housed under controlled conditions: ad libitum access to food and water, a 12-h light/dark cycle, and a constant temperature (22°C) and humidity (45–55%). The rats were acclimatized for one week before the experiment.

### Animal treatment

The adeno-associated virus (AAV)-6 vector-mediated FAM134B overexpression was designed by Genechem (Shanghai, China) and provided in a concentration of $10^{12}$ v.g/mL, of which 150 μL was endotracheally administered to the rats after one week of adaptive feeding. Three weeks after administration of AAV-FAM134B, rats were exposed to hyperoxia to induce HALI.

### Hyperoxia-induced lung injury model

Cages (7 rats per cage) were placed in a hyperoxia exposure chamber for 7 days. The size of the chamber was 635 × 445 × 305 mm and the total flow rates of gases was 5L/min. The bottom of the chamber was lined with a $CO_2$ absorbent (sodium absorbent). Adequate amounts of humidified oxygen were continuously delivered to the confined chamber, and the oxygen concentration was maintained at 90 ± 2% and monitored using an oxygen monitor (ZY-12, China).

### Experiment 1

In Experiment 1, rats were randomly divided into four groups ($n$ = 7): (1) NC group, (2) HALI group, (3) HALI + AAV-FAM134B group, (4) HALI + AAV-FAM134B + LY294002 group. Rats in the fourth group were injected intraperitoneally with LY294002 (5 mg/kg), a potent PI3K inhibitor, dissolved in a solvent consisting of 5% DMSO +40% PEG300 + 5% Tween80 + 50% dd$H_2O$. LY294002 was injected following hyperoxia exposure once daily for 7 days. The air and hyperoxia groups were injected with equal amounts of solvent.

### Experiment 2

In Experiment 2, rats were randomly divided into four groups ($n$ = 7): (1) RA group; (2) RA + $CeO_2$-NPs group; (3) HALI group; and (4); HALI + $CeO_2$-NPs group. Rats in the $CeO_2$-NPs group were intraperitoneally injected with $CeO_2$-NPs (0.5 mg/kg) following hyperoxia exposure once daily for 7 days.

## METHOD DETAILS

### Western blotting

Following normoxic or hyperoxic incubation, we used radioimmunoprecipitation assay (RIPA) buffer (AR0102, Boster) to extract total proteins supplemented with a mixture containing a protease inhibitor (AR1178, Boster) and a phosphatase inhibitor (AR1183, Boster). The BCA Protein Assay Kit (AR1189, Boster) was used to measure the concentration of extracted proteins, and equal amounts of isolated proteins were subjected to sodium dodecyl-sulfate polyacrylamide gel electrophoresis (SDS-PAGE). To facilitate blotting, the size-separated proteins were transferred onto polyvinylidene fluoride (PVDF) membranes (IPVH00010, Millipore). The membranes were blocked with 5% BSA blocking solution (SW3015, Solarbio) and incubated overnight at 4°C with the following primary antibodies: anti-FAM134B antibody (21537-1-AP, Proteintech), anti-LC3B antibody (T55992, Abmart), anti-caspase3 antibody (19677-1-AP, Proteintech), anti-Bax antibody (T40051, Abmart), anti-Bcl-2 antibody (T40056, Abmart), anti-E-cadherin antibody (TA0131, Abmart), anti-N-cadherin antibody (T55015, Abmart), anti-Vimentin antibody (T55134, Abmart), anti-PI3K antibody (T40115, Abmart), anti-P-PI3K antibody (T40065, Abmart), anti-AKT antibody (60203-2-Ig, Proteintech), anti-P-AKT antibody (80455-1-RR. Proteintech), and anti-Beta-actin antibody (GB15003, Servicebio). After washing, membranes were incubated for 1 h with secondary antibodies (SA00001-1-A,SA00001-2, Proteintech) coupled to horseradish peroxidase. The membranes were observed using a membrane imaging device (Clinx, ChemiScope S6), and protein expression was assessed using the ECL western blotting substrate (AR1197, Boster).

### CCK-8 and EdU assays

The cells were plated in 96-well plates at a density of 3000 cells in 100 μL medium per well. Cell viability was quantitatively assessed using a Cell Counting Kit-8 (CCK-8) (C0038, Beyotime) according to the manufacturer's instructions. For the EdU assay, $4 \times 10^4$ cells were cultured in each well of a 24-well plate and examined using an EdU kit (C0071S, Beyotime) according to the manufacturer's instructions.

### Wound-healing assay and transwell migration

Cells were grown to a density of 90–100% and then placed in different environments for culturing after wounding the cells with the tip of a sterile pipette tip. The width of the wound was measured to estimate cell migration. Transwell plates with 8 μm membranes were used to detect transwell migration. After resuspending in serum, $1 \times 10^5$ cells were inoculated in the upper chamber, and 600 μL of complete culture medium was added to the lower chamber.

### Live-cell imaging and transmission electron microscopy

RLE-6TN cells (3000 cells/well) were inoculated in 96-well culture plates. Three randomly selected fields of view were photographed and counted under a phase contrast microscope (Olympus, Japan). Cell counting was performed using a Cytation C5 (BioTek, USA). The physical properties of $CeO_2$-NPs were observed by a Transmission Electron Microscope (TEM; FEI, USA).

### Detection of ROS production

The level of intracellular reactive oxygen species (ROS) was determined using a commercial kit (S0033S, Beyotime) following the manufacturer's instructions. RLE-6TN was incubated with the fluorescent probe 2′,7′-dichlorofluorescein diacetate (DCFH-DA) in the dark for 30 min at 37°C. Next, images were captured using a fluorescence microscope (Olympus, IX73).

### Real-time fluorescence qPCR

The PrimeScript RT Reagent Kit (RR047A, Takara) was used for reverse transcription after extracting total RNA using Trizol reagent (G3013, Servicebio). Quantitative PCR was performed using a real-time PCR detection system (Bio-Rad, CFX96) and TB Green premix Ex Taq (RR820A, Takara). The primers used were as follows:

FAM134B (Forward: 5′-GTACACTCCGCAGACAGACACTTC-3′; Reverse: 5′-TTTGTTCCCGTCCCATTTTCCAGAG-3′); GAPDH (Forward: 5′-ACCACAGTCCATGCCATCAC-3′; Reverse: 5′- TCCACCACCCTGTTGCTGTA-3′).

### Flow cytometry

RLE-6TN cells cultured under different conditions were collected and washed twice with pre-chilled (4°C) phosphate-buffered saline (PBS). Cells were stained using an Annexin V-IF647/PI Cell Apoptosis Detection Kit (G1514, Servicebio) according to the manufacturer's instructions for apoptosis testing. The cells were incubated with Annexin V and PI binding buffer and subjected to flow cytometric analysis. Annexin V was labeled with the fluorescent dye IF647 and used as an assay probe to detect early apoptosis. PI was also used to distinguish surviving cells from necrotic and late apoptotic cells. The combination of Annexin V-IF647 and PI showed negative staining in living cells (Annexin $V^-/PI^-$), mono-fluorescence positivity in early apoptotic cells (Annexin $V^+/PI^-$), and dual fluorescence positivity in late apoptotic and necrotic cells (Annexin $V^+/PI^+$). The apoptosis rate was measured using a flow cytometer (Novo Cyte Advanteon Dx VBR, Agilent Technologies) with its accompanying software.

### Wet/dry lung weight ratio

The upper lobe of the right lung was taken at the end of the experiment, and after determining the wet weight of the lung, it was dried in an oven at 60°C for 48 h. The wet/dry weight ratio was calculated.

### Histopathology of lung tissue

The left lung was fixed in 4% paraformaldehyde for 24 h at room temperature and then embedded in paraffin. The paraffin-embedded lung tissue was cut into 4 μm sections and stained with hematoxylin-eosin (H&E). Samples were analyzed by light microscopy. The degree of lung injury was scored on a scale from 0 to 3: Grade 0, normal pulmonary appearance; Grade 1, Mild to moderate interstitial hyperemia and neutrophil infiltration; Grade 2, perivascular edema formation, partial leukocyte infiltration, moderate neutrophil leukocyte infiltration; Grade 3, Severe structural destruction of the lungs and massive neutrophilic infiltration.

### Immunohistochemistry and immunofluorescence

Lung tissue sections were deparaffinized with xylene, rehydrated in graded alcohol, boiled in 0.01 M sodium citrate buffer (pH 6.0), cooled at room temperature, and washed three times with PBS. Sections were blocked with 3% hydrogen peroxide for endogenous peroxidase and 1% goat serum for 30 min at room temperature. Sections were then incubated with the corresponding primary antibodies at 4°C overnight. Sections were then washed and incubated with rat-specific horseradish peroxidase polymer anti-rabbit antibody for 30 min, followed by the addition of horseradish peroxidase substrate for 3 min. The lung sections were then stained with hematoxylin. For immunofluorescence, enzyme-labeled secondary antibodies were added after washing and incubated for 50 min at room temperature. The sections were then stained with 4′,6-diamidino-2-phenylindole (DAPI). Images were observed under a fluorescence microscope, and the average OD values and fluorescence intensities were calculated using ImageJ software.

### Masson trichrome staining

Lung tissue collagen fiber deposition was detected using Masson staining. Lung tissue sections were deparaffinized with xylene and then rehydrated in graded alcohol solutions. Tissue sections were stained with Masson's Muscle Trichrome Staining Kit (G1340, Solarbio) according to the manufacturer's instructions. After staining, the tissue sections were observed under a light microscope. ImageJ software was used to quantify the areas occupied by collagen (blue), which were then divided by the total area examined (as the percentage of collagen fibers).

### TUNEL staining

Apoptosis of lung cells was evaluated by terminal deoxynucleotidyl transferase-mediated dUTP nick end labeling (TUNEL) staining according to the TUNEL TMR red kit. Lung tissue sections were stained according to the manufacturer's instructions (G1502, Servicebio). Cells containing red particles in the nucleus after staining were considered TUNEL positive. DAPI was used to stain the nuclei. Finally, the fluorescence signal was monitored under a fluorescent inverted microscope (Olympus, IX73). ImageJ software was used to count the fluorescence intensity.

## QUANTIFICATION AND STATISTICAL ANALYSIS

Images were analyzed using ImageJ software. Experimental data were analyzed using GraphPad Prism 9. Normally distributed data are expressed as the mean ± standard deviation (SD), and one-way analysis of variance (ANOVA) was performed to compare the groups. Statistical significance was set at $p < 0.05$. The number of biological replicates is indicated in individual figures.